

# Genesis of Ferromanganese Deposits from the Central Anatolian Province, Yozgat-Aşağı Eğerci Village-TURKEY: Geochemical Properties and Fluid Inclusions

Nursel Öksüz<sup>1,\*</sup> and Sümeyra Kaya<sup>2</sup>

<sup>1</sup> Bozok University, Faculty of Engineering & Architecture, Department of Geological Engineering, 66100 Yozgat, Turkey; (corresponding author: nursel.oksuz@gmail.com)

<sup>2</sup> Bozok University, Graduate Education Institute, 66100 Yozgat, Turkey

doi: 10.4154/gc.2021.20



## Article history:

Manuscript received May 20, 2021

Revised manuscript accepted September 10, 2021

Available online October 27, 2021

**Keywords:** Ferromanganese, rare earth elements, hydrothermal, fluid inclusions, Yozgat (TURKEY)

## Abstract

Eğerci village is located 16 km southwest of Yerköy (Yozgat) area which has a ferromanganese deposit that formed at the contact between basalt and limestone and shows that a banded stockwork structure occurs occasionally within the limestone. The mineralization consists of pyrolusite, goethite, and ramsdellite, together with a lesser quantity of magnetite. Gangue minerals are determined as calcite and quartz. REE data from the mineral samples demonstrate a range from 2.70 - 63.70 ppm and the average value is 28.00. These results permit a comparison to be made with mineralization in hydrothermal deposits. Moreover, mineral samples show a positive Eu anomaly 0.88-48.10 ppm (ave. 9.94 ppm). The Ce anomaly values vary between 0.02 and 0.88 ppm (ave. 0.58 ppm). It is possible that the mineralization may be affected by the mixing of seawater and hydrothermal fluids. The value of the positive Eu anomaly is evidence of modern oceanic hydrothermal manganese deposits. Insight of previous fluid inclusion studies can be easily inferred that mineralization can occur at three different stages. The temperature of the first stage ranged from 338 °C to 428 °C and other stages vary from 269 °C - 317 °C and 143 °C - 236 °C, respectively. As a comparison, calculated salinity is higher in Type I fluid inclusions (1.9-14.7 wt.% NaCl equiv.) than Type II and III fluid inclusions (1.9-5.1 wt.% NaCl equiv.) It is possible that the mineralization was formed by the mixing of magmatic and meteoric waters.

## 1. INTRODUCTION

Manganese deposits in Turkey are divided into four main groups by noting sources, tectonic environments, and structural features (ÖZTÜRK, 1993). These are; 1. Hydrothermal and hydrogenous manganese deposits within radiolarite cherts, 2. Diagenetic deposits related to black shales within Lower Cretaceous carbonates, 3. Hydrothermal deposits within volcano-sedimentary and 4. Sedimentary-derived deposits within Oligocene sediments.

Many manganese formations are observed along a line from west to east in Yozgat province. Most of these are emplaced within ophiolitic units widely observed in the region and are manganese-ferromanganese deposits interlayered with radiolarites. Though some deposits were determined to have very high grades (up to 69.91%), they remain short-term operations due to low reserves. While Si values reach up to 40% in some regions, the Fe content values reach up to 29% (ÖKSÜZ 2011a,b; ÖKSÜZ & OKUYUCU, 2014; ÖKSÜZ, 2018; ÖKSÜZ et al., 2021). The geological, mineralogical, and geochemical assessments of these formations have been the topic of many studies (ÖKSÜZ, 2011a,b; ÖKSÜZ & OKUYUCU, 2014; ÖKSÜZ, 2018; ÖKSÜZ et al., 2021). In those studies, it was determined that Yozgat manganese deposits have three different origins of hydrothermal, hydrogenous, and detrital sources.

The topic of the study is the ferromanganese mineralization observed in the Eğerci region, which was observed to be different from other mineralization in the Yozgat region. This ferromanganese deposit in the region was selected as the research topic as it has not appeared in any previous studies. The basic aims of the study were to define the geology of the region, the ore para-

genesis, wall rocks, the sources of different hydrothermal fluids in the mineralization with ore REE geochemistry, and fluid inclusion studies and to determine a mineralization model for ore deposits in the region.

## 2. GEOLOGICAL SETTING

### 2.1. Regional Geology

The manganese mineralization which forms the topic of the study is observed in Aşağı Eğerci village located 16 km southwest of Yerköy (YOZGAT) county and is situated within one of the most important massifs in Turkey of the Central Anatolian massif. The oldest unit outcropping in the region is the Paleozoic Bozçaldağ Formation (Fig. 1). The unit named by SEYMEN (1982) comprises grey coloured, mostly coarse calcite crystal-rich, moderately-thick bedded marbles, and massive marbles. The massive marbles are observed in a very small area south of Hacılı village in the study area and are cut by an Upper Cretaceous Central Anatolian granite (AKÇAY et al., 2007). The Eocene Boğazköy Formation (ÖZCAN et al., 1980) transgressively overlies intrusives in some regions and older units above an angular unconformity in other regions in the study area and close surroundings. The unit has volcanic interlayers and comprises sandstone, siltstone, some pebblestone, mudstone, and limestone. This formation is divided into three members of the 'limestone member' comprising sandy-silty limestone and massive limestone containing nummulites, corals and gastropod fossils, the 'Alimpinar volcanic member' comprising basalt and basaltic pyroclastic rocks, and the 'dacite member' comprising dominantly dacitic tuffs with occasional dacitic and rhyolitic rocks (ÖZCAN et al., 1980). The dacite member is not observed in the study area. These three

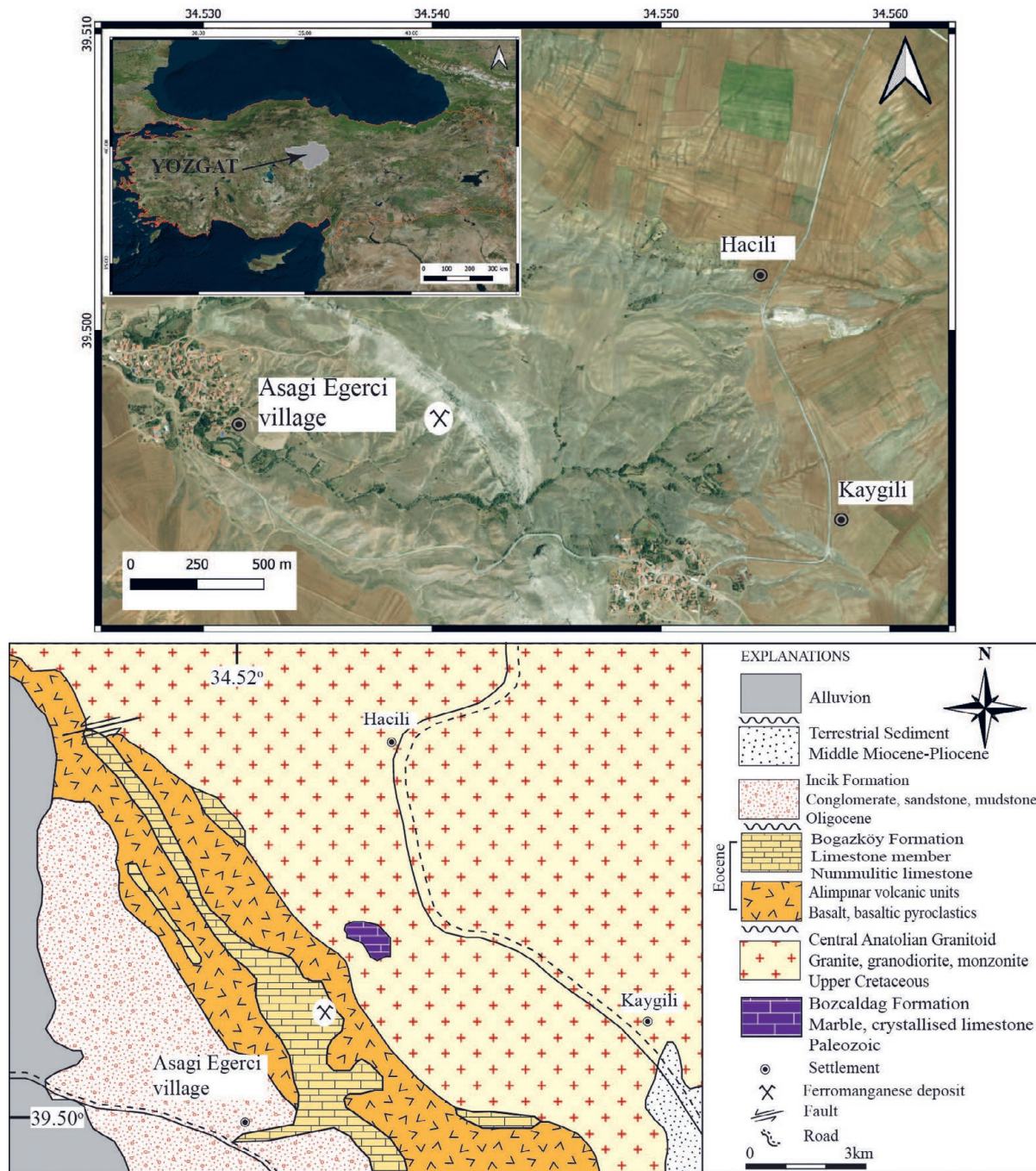


Figure 1. Location and geology map of the study area (modified by AKÇAY et al. 2007).

members identified in the formation have both lateral and vertical transitions with each other. Additionally, the basal structures observed in the Alimpinar volcanic member indicate submarine volcanism. The unit is generally observed in the north-northwest and southeast regions around Aşağı Egerci village. The Oligocene İncik Formation (OKTAY, 1981), is distinguished by dominant pebblestone, sandstone, and mudstone lithologies and formed in a terrestrial environment, while Middle Miocene-Pliocene lacustrine and terrestrial fluvial sediments unconformably overlie all units. The youngest unit in the region is the Quaternary alluvium (KETIN, 1955; AKÇAY et al., 2007).

In the study area, the effects are observed of the Laramian stage of Alpine orogenesis on the intense deformation of central Anatolia and the Taurus (KETIN, 1966). Magmatism covering

large areas of the region occurred as plutonic activity within crystalline massifs, and submarine volcanism in the Upper Cretaceous and Middle Eocene periods. Middle Eocene units represent rocks developed in shallow marine and volcanic facies. In the Lower-Middle Eocene period, the sea level was higher than in the Cretaceous period. Towards the end of the Middle Eocene, the sea gradually began to retreat, lagoons formed, and gypsum and clayey marls formed toward the end of the Middle Eocene. At the end of the Middle Eocene, the sea regressed further and at the same time uplift and erosion occurred, with red conglomeritic units forming in the Oligocene. During the Oligocene, the sea regressed further and lagoons formed. At the end of the Oligocene, occasional fresh and saltwater lakes remained while the sea was fully regressed (KETIN, 1955). Volcanic activity in younger cycles was not observed in the study area (KETIN, 1955).

### 3. SAMPLING AND ANALYTICAL METHODS

A total of 40 ore samples were taken systematically from the ferromanganese mineralization observed in the study area. These samples were separated for geochemical analysis, polished sections, and fluid inclusion studies. Sample powders under 200 mesh were analyzed at the General Directorate of Mineral Research and Exploration (MTA) in Turkey. Major oxide and trace element contents were determined with ICP-ES and REE's were analyzed with the ICP-MS method. Results of the analyses are given in Tables 1 to 3. Polished sections were prepared from 15 samples by the same unit. The polished samples were investigated with a reflected light Leica microscope in Bozok University Laboratory. For accuracy of ore paragenesis, 15 samples had XRD analysis performed in the Bozok University Science and Technology Application and Research Centre (BILTEM).

For fluid inclusion analysis, quartz and calcite samples observed as veins were examined in mineralized samples from the study area. A total of 4 samples had fluid inclusion studies performed. Measurements were performed microthermometrically on double-sided polished sections, using a Linkam THMG-600 heating and cooling stage mounted on an Olympus BX51 microscope in the Recep Tayyip Erdoğan University, Department of Geological Engineering. The equipment was suitable for microthermometric measurements from -196 to 600 °C. The Linksys-32 DV program was used for measurements with 0.1 °C sensitivity and repeated measurements were shown to have an accuracy of ±0.2 °C for freezing and ±1 °C for heating experiments.

### 4. GEOLOGY OF MINERALIZATION

The Boğazköy Formation observed in the region comprises volcanic interlayers, sandstone, siltstone, and lesser amounts of pebble stone, mudstone, and limestone (ÖZCAN et al., 1980). At the base of the unit, poorly defined beds of grey and occasionally red coloured pebblestone and sandstone occur. Above these, there are coal interlayers, light grey in colour, parallel bedded, graded, well-consolidated sandstones and siltstones, and very fine-grained pebblestones. The Eocene Boğazköy Formation is divided into three members; the 'limestone member', 'Alimpınar volcanic member' and 'dacite member'.

The 'limestone member' is commonly observed in the study area and comprises coral, gastropod, and lamellibranchs, grey, moderately-thickly bedded, sandy-silty limestone, and massive limestones (Fig. 2a-c). The unit is widely observed in the region and contains banded and stockwork ferromanganese formations in the study area (Fig. 2c, d-f).

The Alimpınar volcanic member comprises basalt and pyroclastics of basaltic composition. The unit with widespread outcrops in the study area has a lateral transition to the limestone member. Basalts with basal structures indicating submarine volcanism are a purple-black colour, with large glassy minerals, abundant fractures, and joints (Fig. 2c). Pyroclastics are lightly coloured, with uneven erosion surfaces and glass fragments (AKÇAY et al., 2007) (Fig. 2g). The unit has a broad distribution in the study area. Manganese mineralization is observed as bands and occasional stockwork at the contact with limestone and within the limestones (Fig. 2, d-f).

#### 4.1. Ore Petrography

Polished sections of the mineralized samples were investigated with a reflected light microscope. Additionally, XRD analysis

Table 1. Major oxide contents (%) in the ore samples.

Samples%	E-1	E-3	E-6	E-7	E-9	E-10	E-13	E-14	E-15	E-16	E-17	E-18	E-19	E-20	E-21	E-22	E-23	E-24	E-25	E-26	Min.	Max.	Ave.
SiO <sub>2</sub>	0.40	13.90	2.30	8.80	10.40	61.00	35.40	38.50	0.50	12.00	2.50	9.10	11.30	62.00	33.20	37.00	1.50	8.10	11.60	3.90	0.40	62.00	18.17
Al <sub>2</sub> O <sub>3</sub>	0.10	4.00	0.60	0.70	5.50	0.10	0.10	0.10	0.20	3.30	0.40	0.50	5.40	0.10	0.20	0.10	0.30	0.40	0.10	0.50	0.10	5.50	1.14
CaO	50.20	11.70	21.10	4.80	26.90	2.50	15.40	0.40	48.10	12.50	20.00	5.10	27.80	3.50	16.20	0.50	10.00	19.20	3.80	15.40	0.40	50.20	15.76
Fe <sub>2</sub> O <sub>3</sub>	0.1	2.40	0.40	42.10	2.40	14.20	21.50	33.60	0.20	3.40	0.30	43.10	2.50	14.80	21.00	30.50	38.50	2.20	0.50	39.90	0.20	43.10	16.50
K <sub>2</sub> O	0.10	1.90	0.10	0.80	1.70	0.10	0.10	0.10	0.10	1.50	0.20	0.80	1.50	1.70	0.10	1.80	0.30	0.60	0.10	0.10	0.10	1.90	0.69
MgO	0.30	0.80	0.40	1.40	1.00	0.30	0.30	0.40	0.30	0.70	0.20	1.20	0.90	0.20	0.40	0.30	0.20	0.10	0.80	0.60	0.10	1.40	0.54
MnO	9.20	48.40	52.20	26.90	19.40	14.90	11.30	18.00	10.10	45.30	50.90	27.30	20.30	15.10	12.80	19.20	21.50	47.30	55.20	28.00	9.20	55.20	27.67
Na <sub>2</sub> O	0.10	0.10	0.10	0.10	0.40	0.10	0.10	0.10	0.10	0.10	0.20	0.30	0.10	0.20	0.10	0.10	0.20	0.10	0.10	0.30	0.10	0.40	0.15
P <sub>2</sub> O <sub>5</sub>	0.10	0.20	0.40	0.10	0.30	0.10	0.10	0.10	0.10	0.30	0.20	0.40	0.30	0.10	0.20	0.40	0.20	0.10	0.10	0.20	0.10	0.40	0.20
TiO <sub>2</sub>	0.10	0.20	0.10	0.10	0.30	0.10	0.10	0.10	0.20	0.10	0.30	0.10	0.10	0.20	0.30	0.20	0.10	0.10	0.20	0.30	0.10	0.30	0.17
LOI	39.00	16.50	21.90	13.90	23.55	6.40	16.00	0.40	39.00	19.90	24.50	11.70	28.70	1.70	16.40	9.20	24.80	20.00	26.40	9.40	0.40	39.00	18.47
Mn/Fe	101.86	22.31	144.39	0.71	8.94	1.16	0.58	0.59	55.86	14.74	187.71	0.70	8.98	1.13	0.67	0.70	0.62	23.79	122.14	0.78	0.58	187.71	34.92
Al <sub>2</sub> O <sub>3</sub> /TiO <sub>2</sub>	1.00	20.00	6.00	7.00	18.33	1.00	1.00	1.00	1.00	33.00	1.33	5.00	54.00	0.50	0.67	0.50	3.00	4.00	0.50	1.67	0.50	54.00	8.03

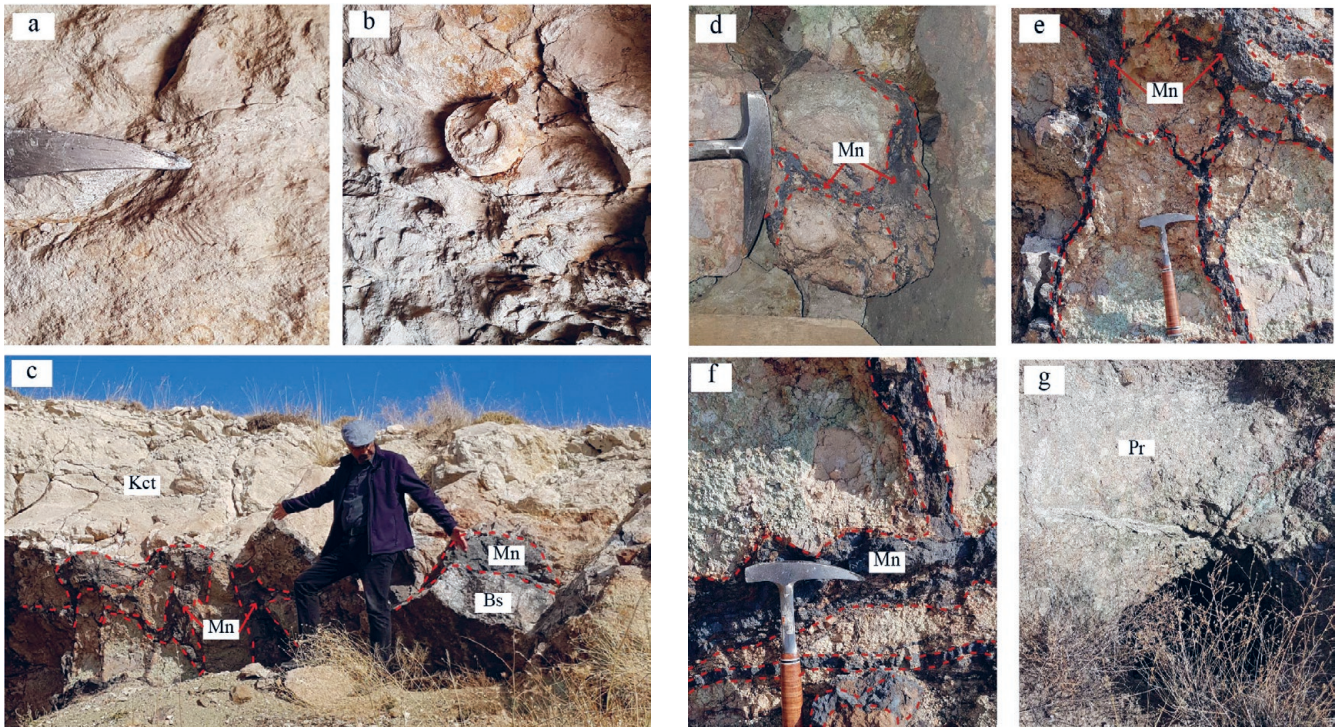


**Figure 2.** a, b. Limestone member: fossiliferous limestone comprising sandy-silty limestone and massive limestones, c. Black basalt with abundant fractures and joints showing basal structures indicating submarine volcanism. Mn: manganese, Bs: basalt; Pr: Pyroclastics, Kct: limestone, d, e, f. Banded and occasionally stockwork mineralization at basalt-limestone contacts and within the limestone. g. Light-coloured pyroclastics with undulating erosion surface.

was performed to support the mineral paragenesis (Fig. 3). Accordingly, the main minerals in the ore paragenesis were pyrolusite, goethite, and ramsdellite. Lesser amounts of magnetite were observed. The gangue minerals comprise calcite and quartz.

Pyrolusite is the most abundant manganese oxide mineral in manganese deposits. There are three different polymorphs of  $MnO_2$ . The most stable and abundant of these is pyrolusite, which is a mineral that may form in both supergene and low-temperature hydrothermal environments and does not infer meaning in terms of origin (NICHOLSON, 1992). Apart from this, other

manganese minerals including ramsdellite and manganite occur in the form of replacements. Pyrolusite formation is typical with weathering developing in terrestrial environments. In this type of mineralization, pyrolusite may contain simple remnant materials from the environment during transport and pyrolusite precipitation generally occurs in carbonate rocks including limestone or dolomite (RAMDOHR, 1980). In environments with a high oxidation potential, pyrolusite may be independent of pH (KRAUSKOPF, 1989). It displays a cream and yellow colour under the first Nicol, while there is cream, yellow, bluish-grey strong

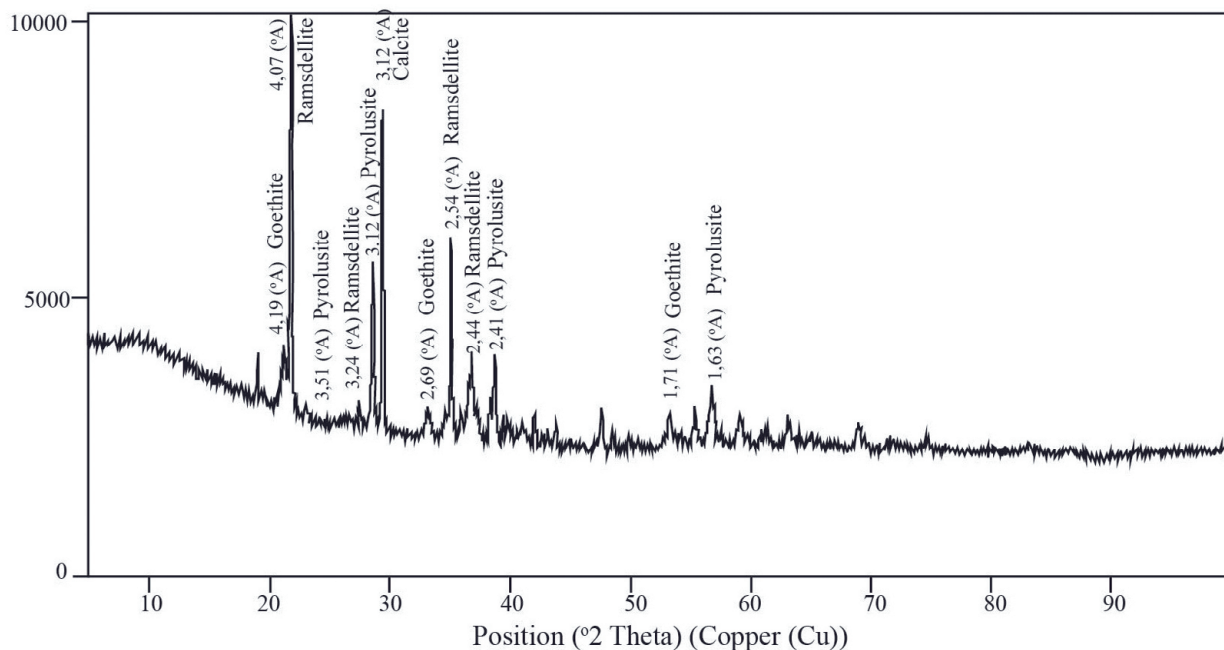


**Figure 3.** X-ray diffractogram for the mineralized samples.

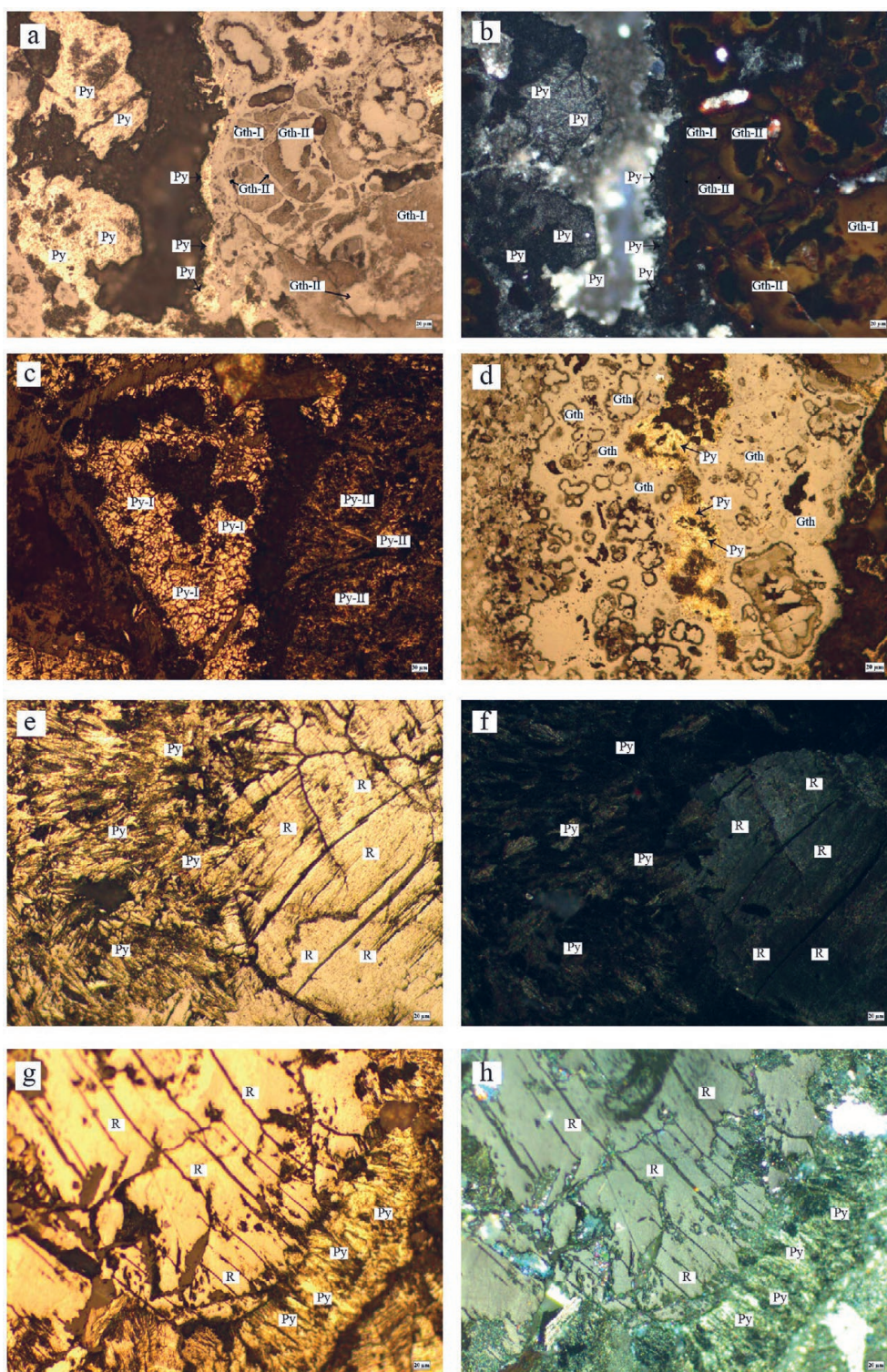


**Figure 4.** Polished section photographs of mineralized samples. a. Cream and yellow goethite replacing pyrolusite and brecciated light and dark grey colour goethite (I Nicol), b. Bluey grey, strongly anisotropic pyrolusite and orange-brown goethite with strong internal reflection (II Nicol). c. Foliation in large-grained (Py-I) and fine-grained pyrolusite (Py-II). d. Fine-grained, vein-fill pyrolusite (I Nicol), light and dark grey goethite with occasional oolite-like texture (I Nicol). e. Cream, bright yellow ramsdellite and pyrolusite were observed replacing ramsdellite (I Nicol). f. Same photograph (II Nicol). Py: pyrolusite, Gth: goethite, R: ramsdellite.

anisotropy under the second Nicol (Fig. 4a, b). There are three different pyrolusite types in the study area (Fig. 4c). One of these is vein fill with small grain size (Fig. 4d), while the other has larger grains in the form of foliation (Fig. 4c, e, f). Additionally, pyrolusites were observed in the form of replacements with ramsdellite (Fig. 4e-h).

Ramsdellite is one of the naturally occurring manganese oxide polymorphs. Due its similarities with pyrolusite, it is very

difficult to make a direct comparison. Though pyrolusite is more commonly observed, ramsdellite may be found in abundant amounts in manganese-rich environments exposed to aqueous alteration at low temperatures (OSTWALD et al., 1984). If the two minerals form together, pyrolusite is notable for its higher sheen. Both minerals are included in the paragenesis of the other, and ramsdellite converts to pyrolusite when heated above 300 °C (RAMDOHR, 1980). This type of transformation is in the form

Table 2. Trace elements contents (ppm) in the ore samples.

ppm	E-1	E-3	E-6	E-7	E-9	E-10	E-13	E-14	E-15	E-16	E-17	E-18	E-19	E-20	E-21	E-22	E-23	E-24	E-25	E-26	Min.	Max.	Ave.
As	15.2	120.0	74.2	412.0	52.6	195.3	206.0	269.5	16.3	125.0	75.5	398.9	55.4	200.3	204.0	280.2	18.3	115.8	78.1	153.3	15.2	412.0	153.3
Be	0.2	1.7	1.0	1.8	0.8	0.1	2.1	0.3	0.2	1.6	0.9	1.8	0.7	0.3	1.9	0.1	1.7	2.3	0.1	1.0	0.1	2.3	1.0
Bi	1.3	18.9	18.1	10.8	3.3	2.8	3.4	8.8	1.2	18.4	17.8	10.4	3.5	2.5	3.4	8.9	1.5	17.5	9.2	8.5	1.2	18.9	8.5
Cd	<0.1	1.2	1.1	17.1	0.2	5.7	7.1	13.0	0.9	1.5	1.2	15.2	0.5	5.8	7.5	12.4	4.2	1.2	1.4	5.4	0.2	17.1	5.4
Co	4.5	45.6	37.1	38.3	19.7	28.5	19.9	22.3	4.2	43.2	36.8	35.2	18.9	29.1	18.4	24.1	4.6	44.9	36.5	26.9	4.2	45.6	26.9
Cu	16.0	229.6	224.9	108.6	55.1	11.4	4.1	<0.1	15.8	223.21	227.2	106.6	54.9	10.8	4.9	0.2	14.9	205.8	190.0	206.3	0.2	223.21	206.3
Ga	2.4	12.7	11.2	10.6	9.8	3.6	7.6	4.6	2.3	11.9	10.9	10.3	9.7	3.3	7.5	4.2	2.1	11.8	10.9	7.8	2.1	12.7	7.8
Ge	0.3	1.2	0.9	5.4	0.7	2.0	2.6	4.2	0.2	1.3	0.8	5.2	0.7	1.9	2.4	4.3	0.3	1.3	0.7	1.9	0.2	5.4	1.9
Hf	<0.1	1.5	0.4	0.2	2.6	<0.1	0.1	0.1	0.1	1.4	0.3	0.2	2.4	0.1	0.1	1.2	0.9	2.2	0.4	0.8	0.1	2.6	0.8
In	<0.1	<0.1	<0.1	<0.1	<0.1	<0.1	<0.1	<0.1	<0.1	<0.1	<0.1	<0.1	<0.1	<0.1	<0.1	<0.1	<0.1	<0.1	<0.1	<0.1	<0.1	<0.1	<0.1
Mo	3.0	38.5	23.1	33.4	20.5	18.2	15.6	21.7	2.9	37.5	22.9	34.2	20.2	17.4	15.4	19.8	20.5	31.2	15.2	21.6	2.9	38.5	21.6
Ni	23.7	91.9	252.1	104.4	61.6	91.2	25.1	16.1	23.4	89.2	245.2	103.2	30.8	90.8	89.5	25.3	17.5	21.5	15.8	74.6	15.8	252.1	74.6
Sb	0.7	3.3	3.1	7.9	1.5	3.6	1.6	3.2	0.6	3.2	3.1	8.1	1.4	3.3	1.4	3.1	0.7	3.6	5.4	3.1	0.6	8.1	3.1
Tl	0.4	0.3	9.9	0.3	0.2	<0.1	<0.1	<0.1	0.4	0.5	8.9	0.2	0.1	0.3	0.1	0.4	0.2	0.1	0.1	1.4	0.1	9.9	1.4
Ba	148.4	3550.1	4750.0	3825.0	930.2	3033.3	6219.1	5406.7	150.2	3670.0	4820.0	3832.0	890.0	3027.0	6315.0	5321.0	2980.0	4520.0	3925.0	3687.9	148.4	6315.0	3687.9
Cr	7.8	40.9	23.4	14.0	53.2	11.5	7.0	10.5	7.6	35.2	22.1	15.1	52.1	10.9	6.9	10.3	8.1	41.2	21.5	21.6	6.9	53.2	21.6
Cs	0.5	0.9	0.2	1.6	1.6	0.1	0.2	0.1	0.4	0.8	0.2	1.5	1.6	0.2	0.1	1.4	0.4	0.8	1.2	0.7	0.1	1.6	0.7
Nb	0.3	2.6	0.8	0.4	5.0	0.1	0.2	0.2	0.2	2.4	0.7	0.4	4.8	0.1	0.3	2.1	3.2	0.1	0.2	1.3	0.1	5.0	1.3
Pb	10.6	64.8	39.9	49.4	39.9	23.5	24.1	40.7	10.5	60.2	38.1	42.5	37.1	22.9	24.5	39.7	9.9	63.9	42.6	36.0	9.9	64.8	36.0
Rb	10.5	58.0	23.0	41.5	54.3	12.3	7.2	8.8	10.4	54.5	23.5	40.9	52.8	11.9	7.5	8.6	9.8	55.2	25.4	27.2	7.2	58.0	27.2
Sr	196.4	823.0	834.5	806.3	321.0	424.0	578.0	494.5	194.5	820.8	850.2	804.1	325.4	425.3	580.5	470.8	205.0	562.2	492.5	537.3	194.5	850.2	537.3
Ta	0.1	0.4	0.2	0.3	0.6	0.6	0.4	0.4	0.1	0.3	0.2	0.4	0.5	0.6	0.4	0.1	0.2	0.3	0.4	0.3	0.1	0.6	0.3
Zr	3.3	73.6	25.7	12.2	134.0	1.2	4.6	3.6	3.2	74.1	24.2	13.5	120.4	1.5	5.1	3.7	3.2	70.5	24.8	31.7	1.2	134.0	31.7
Hf	0.1	1.5	0.4	0.2	2.8	0.1	0.1	0.1	1.5	0.3	0.1	0.2	2.5	1.2	0.1	0.2	2.1	1.2	0.1	0.8	0.1	2.8	0.8
Sc	2.1	5.6	2.6	2.1	7.3	1.6	1.7	1.8	1.9	5.2	2.5	2.2	7.4	1.4	1.2	1.8	2.3	5.1	2.8	3.2	1.2	7.4	3.2
Th	0.7	2.2	0.9	0.8	3.9	0.1	0.3	0.3	0.6	2.1	0.9	3.7	0.1	0.2	0.6	2.7	0.3	0.1	0.4	1.1	0.1	3.9	1.1
U	0.9	7.9	3.0	2.6	3.8	2.4	4.6	9.8	0.8	7.5	2.9	2.5	3.7	2.2	4.4	9.7	0.9	7.4	2.9	4.2	0.8	9.8	4.2
V	30.9	238.5	165.0	281.8	121.3	116.4	31.7	75.4	29.8	234.2	170.8	285.1	119.8	115.4	30.8	74.2	120.2	250.7	28.9	132.7	28.9	285.1	132.7
Co/Ni	0.1	0.5	0.3	0.2	0.7	0.1	0.1	0.1	0.1	0.5	0.3	0.2	0.6	0.1	0.3	1.2	1.4	0.0	0.1	0.4	0.0	1.4	0.4
V/(V+Ni)	23.1	158.5	83.5	64.1	195.6	19.2	39.1	32.4	30.4	160.6	86.4	74.3	185.6	21.0	20.4	3.2	2.3	3595.5	347.2	81.0	2.3	3595.5	261.2
Sr/Ba	1.3	0.2	0.2	0.2	0.3	0.1	0.1	0.1	1.3	0.2	0.2	0.2	0.4	0.1	0.1	0.1	0.1	0.1	0.1	0.1	0.1	1.3	0.3

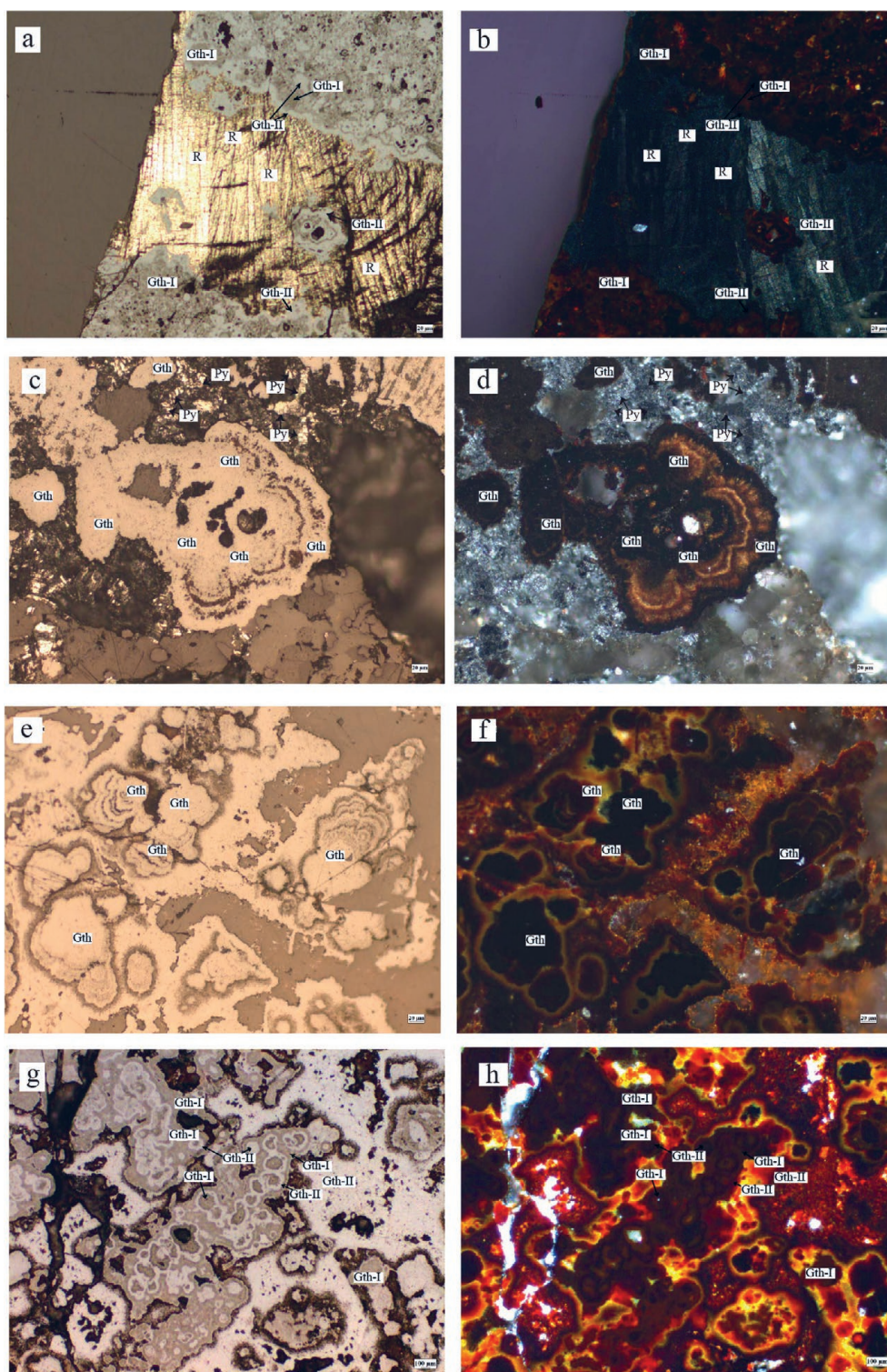


**Figure 5.** Polished section photographs of mineralized samples. a. Ramsdellite in the form of veins within goethite (I Nicol), b. Ramsdellite with strong greenish anisotropy (II Nicol). c. Colloid texture, greyish colour goethite (I Nicol). d. Colloid texture goethite with clear orange internal reflection (II Nicol). e. Colloid texture, greyish colour goethite (I Nicol). f. Colloid texture goethite with clear orange internal reflection (II Nicol). g. Light and dark grey goethite with oolitic texture (I Nicol). h. goethite with oolitic texture showing red and orange internal reflection (II Nicol). Py: pyrolusite, Gth: goethite, R: ramsdellite.

of nested or small pyrolusites observed surrounding ramsdellite in the study area (Fig. 4e-h). Ramsdellite identified with XRD is differentiated from pyrolusite by its greenish-grey anisotropy colour especially (see Fig. 3; Fig. 4f, h; Fig. 5b).

The other mineral commonly observed in mineralization in the study area is goethite. Goethite observed on both XRD and ore microscopy shows the presence of several different stages within the mineralization (Fig. 4a b; Fig. 5c-h). Goethite is ob-

served with different shades of grey under the first Nicol and has typical yellow, orange, and red internal reflection under the second Nicol (Fig. 5d, f, h). In some samples, oolitic textures in goethite are very pronounced (Fig. 5g, h). Though these textures are actually sedimentation textures, similar shapes may form in mineralization developing from solutions and melts in some circumstances. Though the resemblance of these textures to bacteria was discussed at first, later studies state that they represent a hydro-

Table 3. Rare earth elements (REE) contents (ppm) in the ore samples.

Sample ppm	E-1	E-3	E-6	E-7	E-9	E-10	E-13	E-14	E-15	E-16	E-17	E-18	E-19	E-20	E-21	E-22	E-23	E-24	E-25	E-26	Min.	Max.	Ave.
La	2.80	14.00	10.00	6.00	15.20	0.60	2.60	2.00	2.70	13.00	9.90	5.60	15.10	0.50	2.40	1.90	3.00	15.20	2.40	6.57	0.50	15.20	6.57
Ce	2.70	24.30	16.10	11.10	20.80	0.20	2.90	2.00	2.60	24.50	15.80	10.50	19.70	0.40	2.70	2.20	2.40	20.30	0.20	9.55	0.20	24.50	9.55
Pr	0.40	2.30	1.60	1.10	2.60	0.10	0.30	0.20	0.30	2.40	1.30	1.30	2.50	0.10	0.40	0.20	2.10	0.30	1.80	1.12	0.10	2.60	1.12
Nd	1.90	10.10	7.30	4.50	11.30	0.20	1.50	0.80	1.70	10.50	6.40	4.60	10.90	0.20	1.60	0.70	8.90	6.90	1.70	4.83	0.20	11.30	4.83
Sm	0.30	1.80	1.30	0.80	2.00	0.10	0.30	0.10	0.20	1.60	1.20	0.60	1.90	0.10	0.20	0.10	0.30	0.40	0.40	0.72	0.10	2.00	0.72
Eu	0.10	1.40	1.40	1.10	0.80	0.70	1.50	1.20	0.10	1.20	1.40	1.20	0.90	0.60	1.40	1.60	0.90	1.30	0.60	1.02	0.10	1.60	1.02
Gd	0.40	2.00	1.50	1.00	2.10	0.10	0.40	0.20	0.30	1.80	1.40	0.90	2.30	0.10	0.30	0.20	0.40	1.50	0.30	0.91	0.10	2.30	0.91
Tb	0.10	0.30	0.30	0.20	0.40	0.10	0.10	0.10	0.10	0.20	0.30	0.40	0.20	0.10	0.20	0.30	0.10	0.20	0.10	0.20	0.10	0.40	0.20
Dy	0.4	2.40	1.80	1.10	2.40	0.10	0.30	0.10	0.30	2.30	1.70	1.30	2.20	0.10	0.30	0.10	0.30	2.10	1.80	1.15	0.10	2.40	1.15
Ho	0.10	0.50	0.40	0.30	0.50	0.10	0.10	0.10	0.10	0.40	0.30	0.40	0.50	0.10	0.10	0.20	0.30	0.50	0.20	0.27	0.10	0.50	0.27
Er	0.3	1.60	1.20	0.80	1.50	0.10	0.20	0.10	0.30	1.40	1.60	0.70	1.20	0.10	0.20	0.70	0.10	0.20	0.70	0.71	0.10	1.60	0.71
Tm	0.10	0.20	0.20	0.10	0.20	0.10	0.10	0.10	0.10	0.20	0.30	0.10	0.20	0.10	0.10	0.20	0.30	0.10	0.10	0.15	0.10	0.30	0.15
Yb	0.20	1.60	1.30	0.70	1.40	0.10	0.20	0.10	1.10	0.20	1.50	1.20	0.60	1.30	0.10	0.20	0.10	0.30	1.40	0.70	0.10	1.60	0.72
Lu	0.10	0.20	0.20	0.10	0.20	0.10	0.10	0.10	0.10	0.20	0.20	0.10	0.20	0.10	0.10	0.10	0.20	0.10	0.20	0.14	0.10	0.20	0.14
Y	4.20	19.40	15.60	12.00	19.60	0.70	5.10	2.50	4.30	19.20	14.20	12.50	19.80	0.50	5.40	2.40	9.80	4.80	5.50	9.25	0.50	19.80	9.34
ΣREE	9.90	62.70	44.60	28.90	61.40	2.70	10.60	7.20	10.00	59.90	43.30	28.90	58.40	3.90	10.10	8.70	19.40	49.40	11.90	28.04	2.70	62.70	28.00
ΣLREE/ ΣHREE	4.82	6.13	5.46	5.72	6.06	2.38	6.07	7.00	3.17	7.94	4.93	4.67	6.89	0.95	6.21	3.35	9.78	8.88	1.48	5.63	0.95	9.78	5.38
Ce*	0.47	0.83	0.77	0.87	0.65	0.16	0.56	0.51	0.49	0.88	0.79	0.84	0.62	0.37	0.54	0.59	0.24	0.76	0.02	0.69	0.02	0.88	0.58
Pr*	1.01	0.84	0.84	0.89	0.97	2.85	0.82	0.90	0.81	0.85	0.74	1.07	0.97	2.02	1.10	0.92	2.59	0.14	17.61	0.94	0.14	17.61	1.94
Ceanom	-0.32	-0.07	-0.11	-0.05	-0.18	-0.75	-0.25	-0.28	-0.32	-0.04	-0.10	-0.05	-0.20	-0.38	-0.25	-0.21	-0.58	-0.16	-1.39	-0.15	-1.39	-0.04	-0.29
Eu*	0.88	2.18	2.99	3.72	1.14	20.24	13.25	48.10	1.27	2.10	3.23	5.09	1.30	17.35	17.80	36.32	7.95	5.36	4.66	3.83	0.88	48.10	9.94
La <sub>N</sub> /Yb <sub>N</sub>	9.37	5.86	5.15	5.74	7.27	4.02	8.70	13.39	1.64	43.52	4.42	3.12	16.85	0.26	16.07	6.36	20.09	33.92	1.15	6.29	0.26	43.52	10.66
Y/Ho	42.00	38.80	39.00	40.00	39.20	7.00	51.00	25.00	43.00	48.00	47.33	31.25	39.60	5.00	54.00	12.00	32.67	9.60	27.50	33.79	5.00	54.00	33.29
Tb/Yb	2.20	0.83	1.02	1.26	1.26	4.41	2.20	4.41	0.40	4.41	0.88	1.47	1.47	0.34	8.82	6.61	4.41	2.94	0.31	1.26	0.31	8.82	2.55

$$Ce^* = Ce_N / [2/3 La_N + 1/3 Pr_N]$$

$$Eu^* = Eu_{norm} / [2/3 Sm_{norm} + 1/3 Gd_{norm}]$$

$$C_{anom} = \log [3x Ce_N / (2x La_N + Nd_N)]$$

$$Pr^* = Pr_N / (Ce_N \times Nd_N)^{1/2}$$

$$\Sigma LREE = La + Ce + Pr + Nd + Sm + Eu$$

$$\Sigma HREE = Gd + Tb + Dy + Ho + Er + Tm + Yb + Lu$$

thermal source of mineralization (RAMDOHR, 1980; GÖYMEN & KOÇ, 2000). Additionally, goethite in the study area contains widely observed colloidal textures (Fig. 5c-f), which are known to be sedimentation markers (SCHWARTZ, 1951). Goethite, which also shows brecciated structures, is another indicator of sedimentary formation (Fig. 4a, b).

**5. RESULTS**

**5.1. Trace and Major Elements**

Ore samples from the study area had Mn contents of 7.1-42.8 wt% (average 21.4 wt%) and Fe contents of 0.1-30.2 (average 11.0 wt%). The Mn/Fe ratio was 0.6-187.7 (average 34.9) (Table 1). Eğerci village ferromanganese mineralization had Al<sub>2</sub>O<sub>3</sub>/TiO<sub>2</sub> ratios determined as 0.5-54.0 (ave. 8.0) (Table 1).

The samples from the deposit in this study had Co/Ni values above 2 for 4 samples and below 1 for 16 samples (Table 2). Ore sample V/(V+Ni) ratios were below 0.60 for 8 samples, but above 0.60 for 12 samples (Table 2).

The Mo and Co contents in ore samples were 2.90-38.50 ppm (average 21.64 ppm) and 4.20-45.60 ppm (ave. 26.94) in the study area, respectively (Table 2).

The Ba and As concentrations were 148.40-6315 ppm (average 3687.93 ppm) and 15.20-412.00 ppm (ave. 153.29 ppm) in ore samples in the study area, respectively (Table 2). Samples from the study area had Sr/Ba ratios from 0.07-1.32 (ave. 0.28).

The geochemical data for ore samples from the study area were plotted on a Fe-(Ni+Co+Cu)x10-Mn ternary diagram (Fig. 6a; BONATTI et al., 1972). Accordingly, all samples were distributed in the hydrothermal field.

The source diagram determined with the Na/Mg ratio (NICHOLSON 1992) showed that all samples were distributed in the freshwater field (Fig. 6b). Fig. 6c shows the Fe/Ti ratio plotted against Al/(Al+Fe+Mn) (Fig. 6c; BOSTROM et al., 1976).

On the 10xMgO-Fe<sub>2</sub>O<sub>3</sub>-MnO<sub>2</sub> (CONLY et al., 2011) ternary diagram, ore samples were distributed in the marine hydrothermal, continental hydrothermal, marine hydrogenetic and freshwater hydrogenetic fields (Fig. 6d).

**5.2. REE Geochemistry**

The REE content of samples was used to assess the geochemical parameters of ore mineralization in the study area. REE, commonly used for assessing sources, were analyzed in 20 ore samples taken from the study area. Analysis of the results and some calculations are given in Table 3. ΣREE data had values from 2.70-62.70 ppm with an average (ave.) 28.00 ppm. Additionally, the LREE/HREE ratio in ore samples from the study area was 0.95-9.78 (ave. 5.38) and this value shows that LREE values were enriched compared to HREE values. This enrichment is 0.31-8.82 (ave. 2.55) ratios (Fig. 7). Additionally, Eu and Ce anomalies were assessed. REE data were normalized to chondrite and plotted on spider diagrams (Fig. 7). As seen on the spider diagram for the Eu anomaly, there is a high positive anomaly (Fig. 7). When anomaly values are calculated with the formula  $Eu^* = Eu_N / [2/3Sm_N + 1/3Gd_N]$ , apart from one sample, all displayed a high positive anomaly (0.88-48.10, ave 9.94) (Table 3). In some situations, La enrichment causes false-negative Ce anomalies (BAU & DULSKI, 1999; KATO et al., 2006; PLANAVSKY et al., 2010). For this reason, the Ce\* anomaly is determined with two different calculations.  $Ce^* = Ce_N / [2/3La_N + 1/3Pr_N]$  and  $Pr^* = Pr_N / (Ce_N \times Nd_N)^{1/2}$  calculations were performed. With Ce\* calculations, negative anomalies were supported for all samples (0.02-

**Table 4.** Microthermometric fluid inclusion data from Eğerci village ferromanganese ore samples.

Sample No	Mineral	Vapor Ratio	FI Types	Homog. Mode	Te, °C	Tm-ice, °C	Th, °C	Salinity (wt% NaCl equiv.)		
E-1	Quartz	5-20	Type III	Liquid	-33.8	-2.3	176	3.9		
			Type III	Liquid	-37	-2	216	3.4		
		5-20	Type III	Liquid	-37.7	-1.7	186	2.9		
			Type III	Liquid	-37.6	-1.2	191	2.1		
		5-20	Type III	Liquid	-42.6	-1.3	205	2.2		
			Type I	Vapor		-1.4	354	2.4		
		5-20	Type III	Liquid		-1.4	163	2.4		
			Type III	Vapor	-45.4	-6.4	422	9.8		
		5-20	Tip III	Liquid	-34.1	-1.7	227	2.9		
			Type III	Liquid	-44.7	-2.4	236	4.0		
		30-60	Type I	Vapor	-47.8	-5.6	382	8.7		
			Type I	Vapor	-33.8	-1.5	347	2.6		
		20-30	Tip II	Liquid	-36.9	-1.4	298	2.4		
			E-2	Quartz	Type III	Liquid	-34.8	-1.6	221	2.7
5-20	Type III	Liquid			-40	-1.1	231	1.9		
	Tip II	Liquid			-34.5	-1.1	304	1.9		
5-20	Type III	Liquid			-46	-1.6	217	2.7		
	Type II	Liquid				-1.6	269	2.7		
20-30	Type II	Liquid			-38.1	-1.7	301	2.9		
	Type III	Liquid				-1.6	191	2.7		
5-20	Type III	Liquid			-37.3	-1.8	209	3.1		
	Type I	Vapor				-1.1	346	1.9		
30-60	Type I	Vapor				-1.5	377	2.6		
	Type III	Liquid					187			
E-3	Quartz	30/60			Type I	Vapor	-40.8	-6.1	397	9.4
					Type I	Vapor		-5.4	361	8.5
		30-60			Type I	Vapor	-44.2	-6.2	374	9.6
			Type I	Vapor	-46	-7.3	431	11.0		
		30-60	Type I	Vapor	-49.9	-5.9	338	9.2		
			Type I	Vapor		-7.9	401	11.7		
		30-60	Type I	Vapor		-6	411	9.3		
			Type I	Vapor	-47.3	-8.1	417	12.0		
		30-60	Type I	Vapor		-9.4	438	13.5		
			E-4	Quartz	40-60	Type I	Vapor	-43.3	-1.3	367
Type I	Vapor	-46.8				-10.5	406	14.7		
20-30	Type II	Liquid				-1.4	319	2.4		
	Tip III	Liquid				-2	143	3.4		
40-60	Type I	Vapor				-1.4	376	2.4		
	Type I	Vapor				-1.5	394	2.6		
40-60	Type I	Vapor				-3.8	362	6.2		
	Type II	Liquid				-2.9	277	4.8		
20-30	Type II	Liquid				-2.4	296	4.0		
	Type II	Liquid				-3.1	284	5.1		
40-60	Type I	Vapor		-2.4	388	4.0				

0.88, ave 0.58) (Table 3). As a result of Pr\* calculation, though 6 samples were observed to have a positive anomaly, 14 samples were observed to have a negative anomaly, and the negative anomaly observed in most samples supports the Ce\* calculations (Table 3).

Ce<sub>anom</sub> data were calculated with the formula  $Ce_{anom} = \log(3Ce_N / (2La_N + Nd_N))$  (WRIGHT et al., 1987). When data from

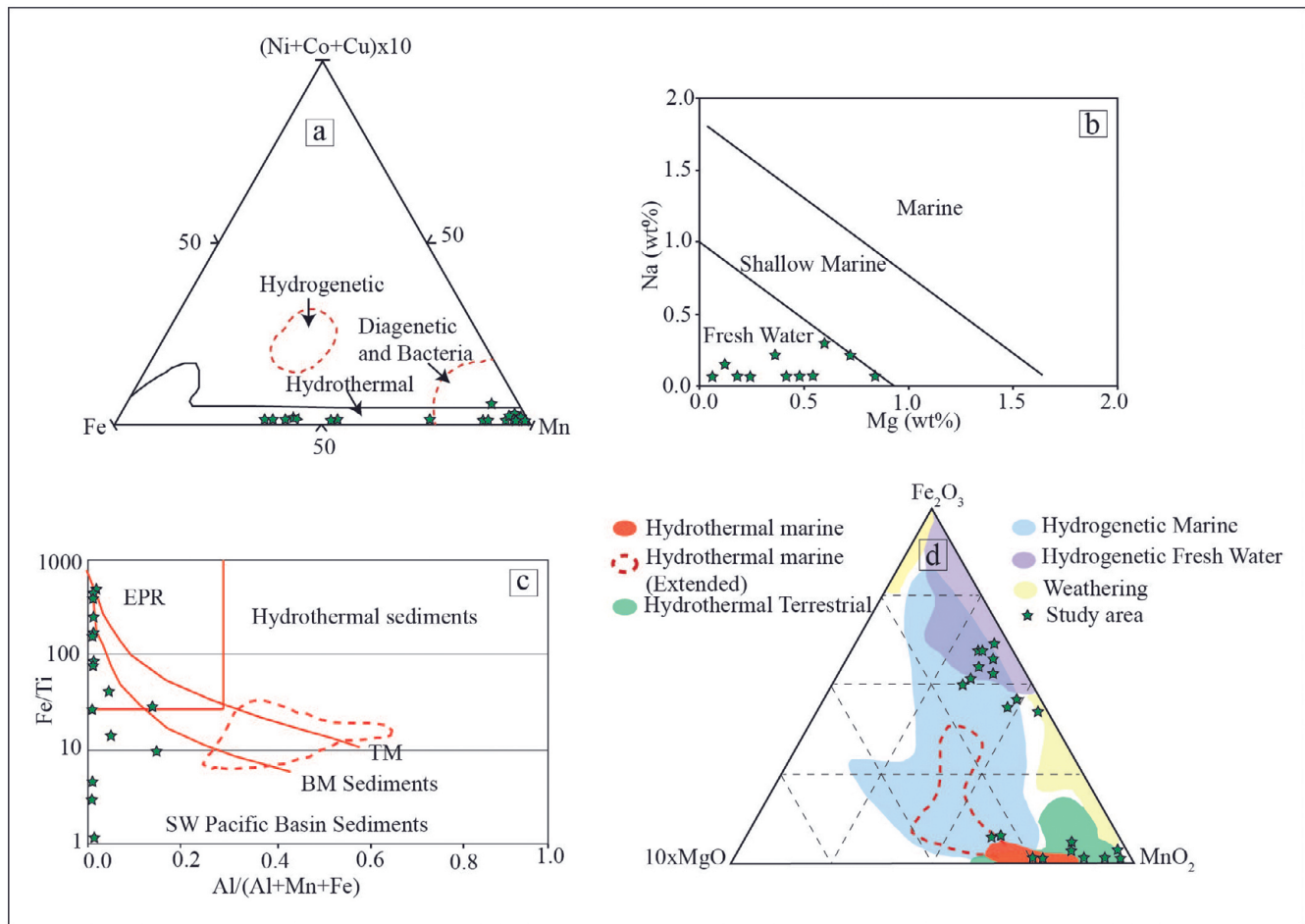


Figure 6. Discrimination diagram of the Egerci ferromanganese mineralization.

(a) Fe-(Ni+Co+Cu)x10-Mn ternary diagram (BONATTI et al., 1972); (b) Na/Mg bivariate diagram (NICHOLSON, 1992); (c) Fe/Ti vs. Al/(Al+Fe+Mn) bivariate diagram (BOSTROM et al., 1976); (d) 10xMg-Fe<sub>2</sub>O<sub>3</sub>-MnO<sub>2</sub>-ternary diagram (CONLY et al., 2011).

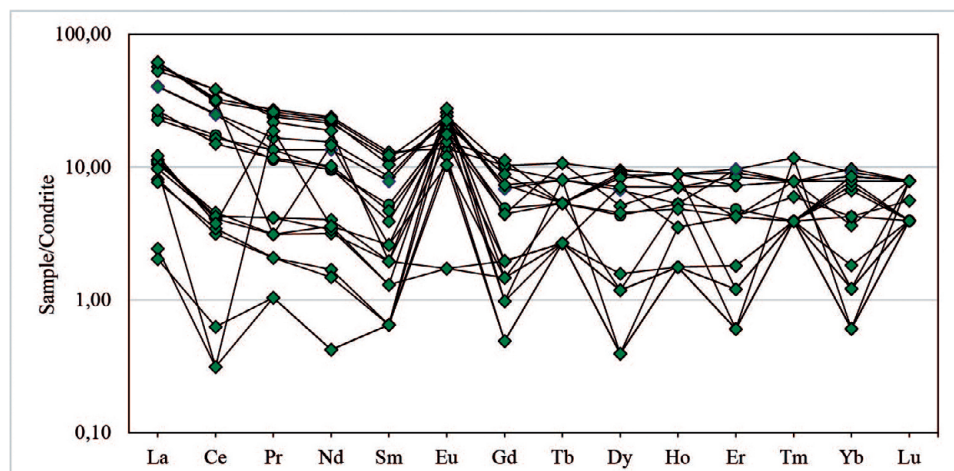


Figure 7. Chondrite normalized REE diagram for ore samples (Normalization values are from EVENSEN, 1978).

the study area are noted, fifteen samples had values smaller than -0.1, while five samples had values larger than -0.1 (Table 3).

In the Egerci village ferromanganese deposits, the Y/Ho ratio was determined to be 33.29 (Table 3).

### 5.3. Fluid Inclusion Petrography and Microthermometry

Fluid inclusion studies were performed on four samples taken from quartz veins with nearly 1 cm thickness located within car-

bonate rocks in the Egerci village ferromanganese mineralization. Along the veins, quartz crystals grow from the surfaces of the wall rock towards the centre of the veins, and they have zoned growth structures (Fig. 8a). In this structure, twinned growth zones are found symmetrically on both sides of the veins, and in the final stage, quartz crystals fill the cavity in the centre of these growth zones. Accordingly, zone 1 and zone 2 correspond to the stage I and stage II quartz formations, respectively, while the final stage quartz filling in the centre is equivalent to 3<sup>rd</sup> stage

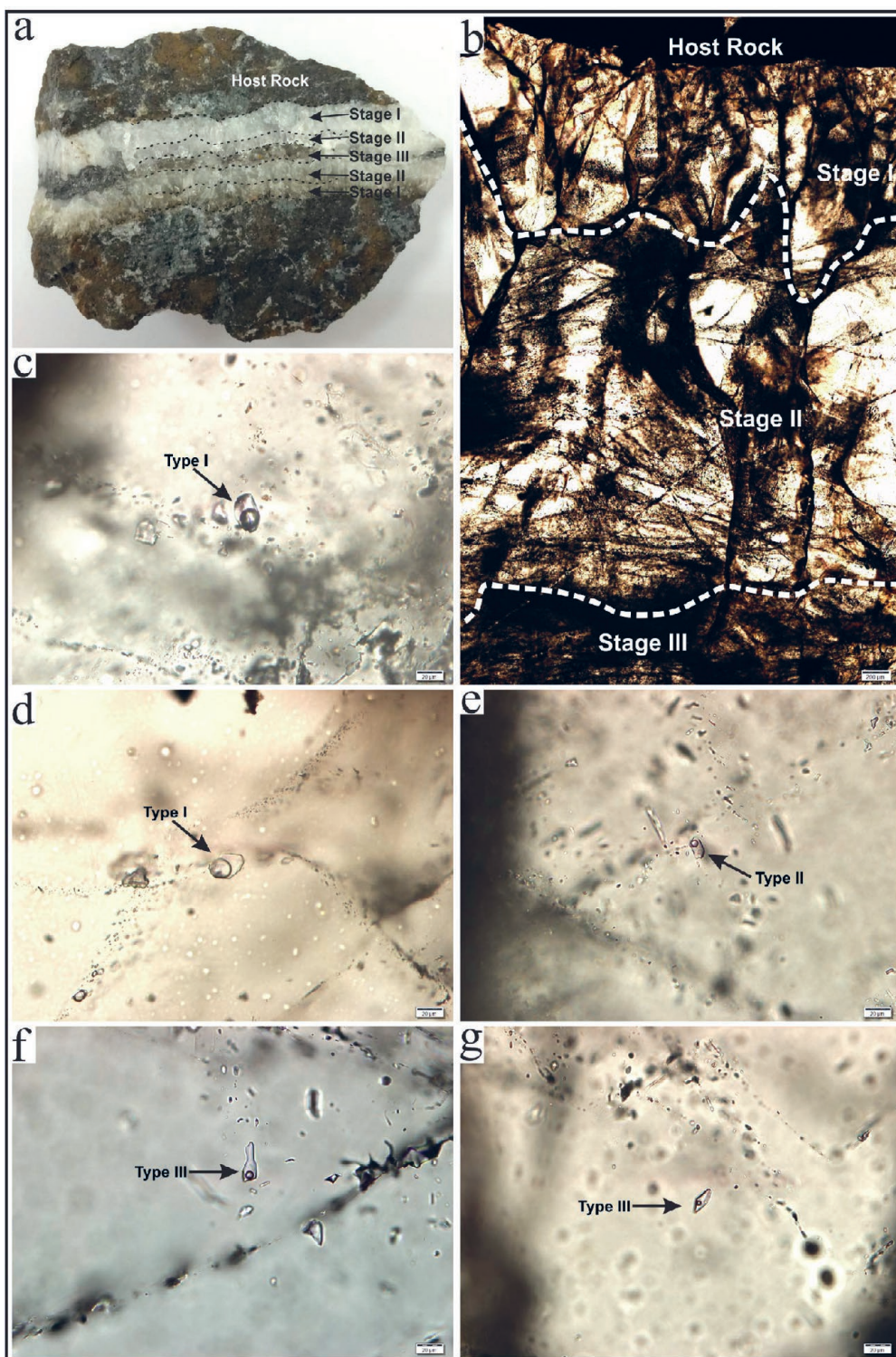


**Figure 8.** a. Growth zonation of the quartz vein in the carbonate host rock, b) Photomicrograph of the quartz crystals with zoned structure, c, d) Type I fluid inclusions in the growth zone I, e) Negative crystal-shaped Type II fluid inclusion in the growth zone II, f) Irregular shaped Type III fluid inclusion in the final stage quartz vein, g) Negative crystal-shaped Type III fluid inclusion in the last stage quartz vein.

quartz formation (Fig. 8b). Eutectic temperatures ( $T_e$ ), final ice melting temperatures ( $T_{m-ice}$ ), and homogenization temperatures ( $T_h$ ) of the fluid inclusions from each zone were measured by the microthermometric study, and the results are presented in Table 4. Eutectic temperatures and final ice melting temperatures of some fluid inclusions could not be measured due to the inclusion size being very small and not being sufficiently transparent. Additionally, the salinity of these inclusions, equivalent to wt.% NaCl were calculated using the  $T_{m-ice}$  values with the

equation proposed by BODNAR (1993) with results reported in Table 4. The blank rows in Table 4 are equivalent to parameters that could not be measured.

According to this, three main fluid inclusion types were identified along the three different growth zones of the samples. Type I fluid inclusions are generally observed to have irregular geometric shapes and rarely tube shapes (Fig. 8c). In some cases, negative crystal-shaped inclusions were also observed (Fig. 8d). The Type I fluid inclusions in zone 1 had sizes from 20 to 30  $\mu\text{m}$ . These fluid

Table 5. Major and trace element contents of various types of manganese and ferromanganese deposits.

Number of samples	7		28		22		15		13		11		14		7		13		23		10		20		20	
	China		Waziristan		Hazara		Bela		Zhub		Sorkhvand		Wakasa		Ulukent		Binkilic		Cayirli		Kasimaga		Eymir		Turkey	
Region	Guichi	Sedimentary	Volcano-sedimentary	Hydrothermal-Hydrogenous	Submarine hydrothermal	Sedimentary	Sedimentary	Sedimentary/diagenetic	Volcano-sedimentary	Volcano-sedimentary	Volcano-sedimentary	Hydrothermal-Hydrogenous														
SiO <sub>2</sub> (%)	(-)	43.69	9.41	46.21	(-)	40.82	58.16	13.68	10.65	63.02	13.43	18.17														
TiO <sub>2</sub> (%)	(-)	0.32	0.84	0.53	0.34	0.03	0.04	0.10	0.02	0.03	0.10	0.17														
Al <sub>2</sub> O <sub>3</sub> (%)	(-)	0.73	12.53	1.86	0.80	0.48	0.55	2.49	2.85	0.65	2.95	1.14														
Fe <sub>2</sub> O <sub>3</sub> (%)	(-)	2.96	20.33	9.85	5.75	2.29	0.92	3.72	2.46	0.68	14.33	16.50														
MnO (%)	(-)	45.88	33.78	32.99	42.46	39.47	32.50	63.78	33.39	29.22	40.43	27.67														
MgO (%)	(-)	0.60	0.59	0.72	0.18	0.07	0.19	1.99	1.27	0.20	12.72	0.54														
CaO (%)	(-)	1.28	6.43	1.44	0.75	0.52	4.15	4.05	18.96	0.24	6.82	15.76														
Na <sub>2</sub> O (%)	(-)	0.29	0.07	0.40	0.30	0.03	0.04	0.24	0.39	0.05	0.06	0.15														
K <sub>2</sub> O (%)	(-)	0.22	0.88	0.58	1.27	0.06	0.10	0.05	0.56	0.11	0.19	0.69														
P <sub>2</sub> O <sub>5</sub> (%)	(-)	0.25	3.73	0.23	0.13	0.06	0.10	0.18	0.31	0.04	0.08	0.20														
Ba (ppm)	212.56	415.00	6304.00	(-)	(-)	1038.34	13.79	427.00	6892.00	1229.40	2719.40	3687.93														
V (ppm)	167.86	144.00	573.00	(-)	(-)	30.68	258.00	(-)	106.00	143.70	106.10	132.68														
Cr (ppm)	107.21	46.00	247.00	37.27	(-)	(-)	10.00	(-)	26.00	13.70	10.00	21.60														
Co (ppm)	4.77	11.00	404.00	21.20	125.38	33.35	2.00	13.00	59.00	25.21	49.50	26.94														
Ni (ppm)	89.39	36.00	305.00	17.93	288.46	98.61	28.00	10.00	167.00	69.40	23.00	74.65														
Cu (ppm)	31.03	72.00	375.00	101.00	20.45	161.18	50.00	56.00	26.00	154.90	126.80	206.27														
Zn (ppm)	137.36	64.00	580.00	71.07	230.94	64.12	26.00	70.00	49.00	66.70	63.50	(-)														
Pb (ppm)	16.49	49.00	2357.00	53.33	464.68	6.56	112.00	65.00	(-)	6.50	53.50	36.04														
Th (ppm)	(-)	2.00	31.00	(-)	(-)	0.28	2.00	(-)	(-)	0.40	433.20	1.10														
Rb (ppm)	37.89	2.00	24.00	(-)	(-)	3.60	2.00	(-)	(-)	2.90	5.00	27.16														
Sr (ppm)	741.34	(-)	(-)	(-)	(-)	667.65	85.00	185.00	2100.00	243.40	255.00	537.32														
Y (ppm)	21.75	(-)	(-)	(-)	(-)	0.27	5.00	(-)	15.00	33.00	22.20	9.34														
Nb (ppm)	6.70	(-)	(-)	(-)	(-)	0.27	3.00	(-)	(-)	0.70	11.10	1.27														
Zr (ppm)	(-)	(-)	(-)	(-)	(-)	5.87	12.00	(-)	32.00	4.00	26.90	31.71														
Mn/Fe	(-)	199.00	2.16	0.27	105.46	115.47	39.00	18.98	15.03	97.17	12.02	34.92														
Al <sub>2</sub> O <sub>3</sub> /TiO <sub>2</sub>	(-)	2.28	14.92	3.49	2.35	15.53	13.75	24.90	142.50	21.67	29.50	8.03														
Co/Ni	0.05	0.31	1.32	1.61	0.45	0.81	0.07	1.30	0.35	0.36	2.15	0.61														
Co/Zn	0.03	0.17	0.70	0.37	0.57	0.81	0.08	0.19	1.20	0.38	0.78	(-)														

(-): There is no analysis

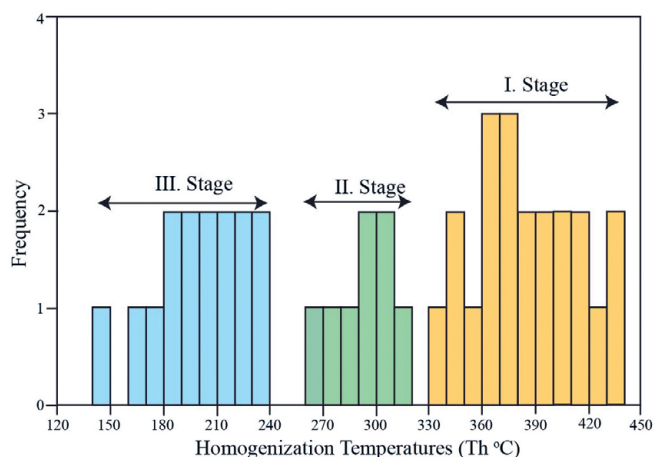


Figure 9. Th histogram for all fluid inclusions in samples.

inclusions have two phases and contain fluid and vapour, and vapour rates vary between 40 and 60% (Fig. 8c, d). These inclusions are isolated from the other fluid inclusions, and they are homogenized into the gas phase during the heating process.

The eutectic temperatures of these inclusions were measured between  $-33.8$  and  $-49.9$  °C. When comparing these  $T_e$  temperatures with the specific eutectic temperatures of the different salt compositions, Type I inclusions were very close to those for inclusions with composition in the  $H_2O$ - $MgCl_2$ - $FeCl_2$ - $CaCl_2$  system (ROEDDER, 1984; SHEPHERD et al., 1985) (Fig. 10). The final ice melting temperatures of Type I inclusions were measured between  $-1.1$  to  $-10.5$  °C. According to these values, the salinity of these inclusions was calculated to vary from 1.9 to 14.7 wt. % NaCl equiv. according to BODNAR (1993). The homogenization temperatures for Type I fluid inclusions were measured as 338 to 438 °C.

Type II fluid inclusions were observed in growth zone 2 in the samples (Fig. 8a, b). These are two phase liquid-rich inclusions, and vapour/liquid ratios vary between 20-30 %. Type II fluid inclusions are generally irregular, but ellipsoidal, tubular, and negative crystal shapes were also defined (Fig. 8e). The inclusion sizes are highly variable, ranging from 10 to 50  $\mu m$ . During microthermometric measurements, Type II fluid inclusions homogenized in the liquid phase. The  $T_e$  temperatures were measured

between  $-34.5$  and  $-38.1$  °C, which correspond to the  $H_2O$ - $FeCl_2$ - $MgCl_2$  fluid salt systems according to SHEPHERD et al. (1985). The  $T_m$ -ice temperatures of Type II inclusions were measured in the range of  $-1.1$  to  $-3.1$  °C. The salinities calculated according to these values range from 1.9 to 5.2 wt. % NaCl equiv. Type II fluid inclusion had  $T_h$  temperatures varying from 269 to 319 °C.

Type III fluid inclusions were found in the centre of the quartz zones equivalent to the final growth stage (Fig. 8a, b). In addition to irregular geometric shapes (Fig. 8f), tubes, and negative crystal shapes (Fig. 8g) are present. These negative crystal shapes support that these inclusions are primary in origin. Their sizes vary from 10 to 30  $\mu m$ . The vapour/liquid ratio ranges from 5 to 20% (Fig. 8f, g) and homogenization of Type III inclusions occurred in the liquid phase. Eutectic temperatures of the Type III inclusions were very close to the Type II inclusions (between  $-33.8$  and  $-46$  °C). Therefore salt compositions of the  $H_2O$ - $FeCl_2$ - $MgCl_2$  system, similar to the Type II inclusions, were also defined for the Type III inclusions. The  $T_m$ -ice temperatures varied from  $-1.1$  to  $-2.4$  °C, corresponding to the salinity range from 1.9 to 4.0 wt.% NaCl equiv. for the Type III inclusions. Homogenization temperatures of these inclusions were measured between 143 to 236 °C (Table 4).

## 6. DISCUSSION

Mineralization in the study area was investigated with field and geochemical studies and the source was interpreted. Major and trace element concentrations and the behaviour of these elements (associations) are frequently used in manganese and ferromanganese deposits (ÖKSÜZ, 2011b; POLGARI et al., 2012; ZARASVANDI et al., 2013). Fe/Mn ratios of the manganese and ferromanganese deposits have been calculated by various studies in the Alpine-Himalaya belt in Turkey and the world (CHOI & HARIYA 1992; ÖZTÜRK 1993; GÜLTEKİN 1998; KOÇ et al., 2000; XIE et al., 2006; SHAH & MOON, 2007; KARAKUŞ et al., 2010; ZARASVANDI et al., 2016; NAREGO et al., 2019; KHAN et al., 2020). Our results display some similarities with the manganese deposits of Guichi (China, XIE et al., 2006), Waziristan (Pakistan, SHAH & MOON, 2007), Hazara (Pakistan, SHAH & MOON, 2007), Bela (Pakistan, NAREJO et al., 2019), Zhob (Pakistan, KHAN et al., 2020), Sorkhvand (Iran, ZARASVANDI et al., 2016), Wakasa (Japan, CHOI & HARIYA, 1992), Ulukent (Turkey, ÖZTÜRK, 1993), Binkılıç (Turkey, GÜL-

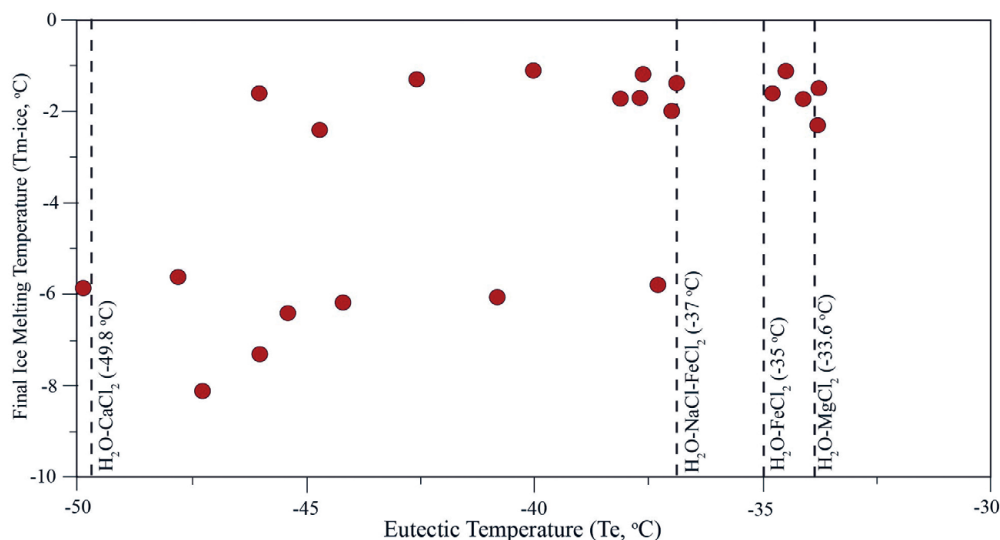
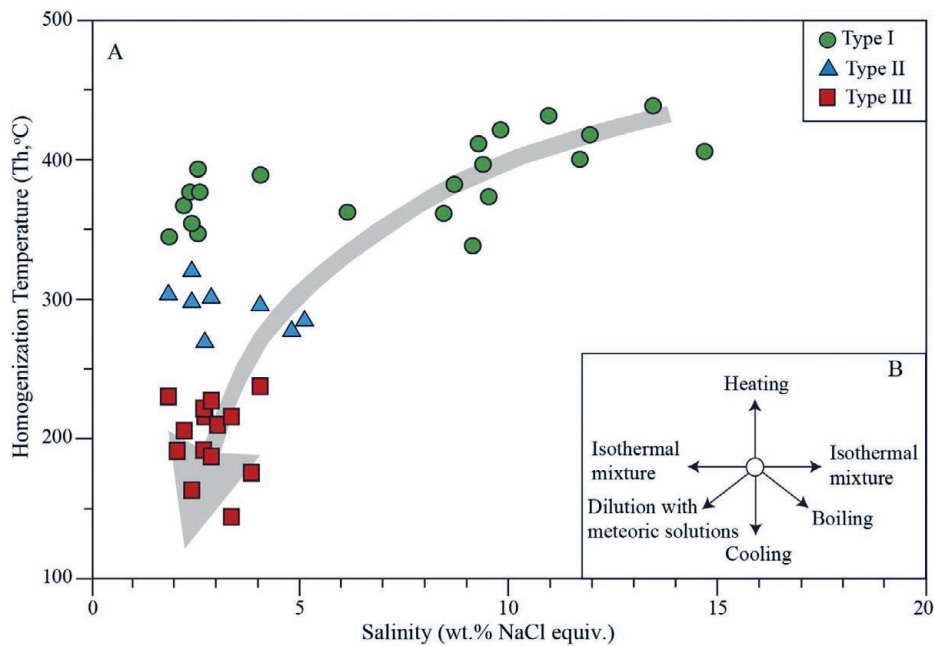


Figure 10.  $T_e$  temperatures and equivalent salinity for all fluid inclusions in samples.



**Figure 11.** A. Th-salinity relationships for all fluid inclusions in samples. B. Comparison of variation in Th-salinity with solution behaviour in a variety of environments.

TEKIN, 1998), Çayırılı (Turkey, KARAKUŞ et al., 2010), Kasımağa (Turkey, KOÇ et al., 2000) and Eymir (Turkey, OKSUZ 2011a) in terms of the mineralizations. Accordingly, the average Mn/Fe ratios in the manganese and ferromanganese deposits of Waziristan, Bela, Zhob, Sorkhvand, Çayırılı, Kasımağa, and Eymir in the ophiolite belt manganese mineralizations are 199.00, 0.27, 105.46, 115.47, 97.17, 12.02, 880.33 respectively (Table 5). In addition, the obtained results are very closely related to the manganese mineralizations of these deposits in Turkey and the world. According to this data, the Eğerci village ferromanganese deposit is compatible with hydrothermal exhalative manganese deposits discovered near submarine spreading centres (NICHOLSON, 1992). In addition, the average Mn/Fe ratios in People Services are now able to provide us with a monthly staff list which includes our AL colleagues the Guichi, Ulukent, and Binkılıç regions indicates that the manganese formations were formed from a sedimentary origin. The Mn/Fe ratios were calculated as 18.98 and 15.03 in Ulukent and Binkılıç regions, respectively (Table 5). The average Mn/Fe ratios are not informative since Mn-Fe relationships are defined as  $Mn/Fe < 1$  for the lacustrine environment,  $Mn/Fe = 1$  for the hydrogenous origin, and  $0.1 < Mn/Fe < 10$  for SEDEX deposits (NICHOLSON et al., 1997).

The  $Al_2O_3/TiO_2$  ratio in sediments indicates a significant degree of volcanic matter contribution in spite of a lower effect from sediment transport or diagenesis (HAYASHI et al., 1997; SUGITANI et al., 1996). The  $Al_2O_3/TiO_2$  ratio in volcanic rocks is between 8–21 (HAYASHI et al., 1997; SUGITANI et al., 1996).  $Al_2O_3/TiO_2$  ratios in Waziristan, Bela, and Zhob deposits were calculated as 2.28, 3.49, and 2.35, respectively (Table 5). In addition, the values observed in Hazara, Sorkhvand, Wakasa, Ulukent, Binkılıç, Çayırılı, Kasımağa, and the Eymir regions are quite high as 14.92, 15.53, 13.75, 142.50, 21.67, 29.50, and 32.53, respectively (Table 5).  $Al_2O_3/TiO_2$  ratio in the study area also shows high values. The ratio shows significant effects of volcanic activity on ore formation in the Eğerci village ferromanganese deposits.

Variable characteristics of Co are closely related to Ni. The Co/Ni ratio is commonly used to understand ore formation processes in manganese deposits (DELIAN, 1994; FERNANDEZ &

MORO, 1998). Especially when deciding on sedimentary environment and sedimentation, it is a guide for hot water sedimentation on the seafloor (TOTH, 1980). According to this data, a Co/Ni value  $< 1$  indicates a sedimentary source (DELIAN, 1994; FERNANDEZ & MORO, 1998), while Co/Ni  $> 1$  indicates a deep marine environment (DELIAN, 1994; NAYAN et al., 1994). Co/Ni ratios in Guichi, Waziristan, Zhob, Sorkhvand, Wakasa, Binkılıç, and Çayırılı regions are 0.05, 0.31, 0.45, 0.81, 0.07, 0.35 and 0.36, respectively, and are lower than 1 (Table 5). In addition, it was observed greater than 1 in Hazara, Bela, Ulukent, Kasımağa, and Eymir regions (1.32, 1.61, 1.30, 2.00, 1.54, respectively). Since this value is both below and above 1 in the ferromanganese deposits of Eğerci village, it is thought that both deep sea and sedimentary environments may be effective in the formation.

According to HEIN et al. (2008), high Ba and minor Co, Ni and Cu contents in manganese oxides show leaching from organic-rich sediments or precipitation of barite at depth in hydrothermal systems. Due to the effect of sedimentation and volcanic activity, the Ba concentration in hydrothermal solutions is higher than seawater (MONNIN et al., 2001). Similarly, Ba contents showed high values in Waziristan, Hazara, Sorkhvand, Ulukent, Binkılıç, Çayırılı, Kasımağa, and the Eymir regions where the sedimentary contribution is intense (415.00, 6304.00, 1038.34, 427.00, 6892.00, 1229.40.00, 2719.40, 2364.70, 3687.93, respectively). According to the very high Ba content, the study area is characterized by mineralization with hydrothermal formation. High As content is a marker of sediment input to hydrothermal manganese (NICHOLSON, 1992). As enrichment in the study area was 15.20–412.00 ppm (ave. 153.29 ppm) (Table 2). This enrichment may be a marker of hydrothermal fluids (ŞAŞMAZ et al., 2014).

When the Sr/Ba ratio is examined, if this ratio is larger than 1, the environment is marine; if it is lower than 1, it indicates the presence of continental freshwater in the formation (XIE et al., 2006; XU et al., 2011). This ratio is variable in sedimentary Mn deposits (DOE et al., 2013). In Mn deposits with hydrothermal effects, it is  $< 0.01$  (DOE et al., 2013). Samples from the study area had Sr/Ba ratio values of 0.07–1.32 (ave. 0.28). Apart from two

samples, all ore samples had a Sr/Ba ratio lower than 1 representing formation in a continental sedimentary environment for mineralization in the study area.

Vanadium is a very stable element during alteration (JIANCHENG et al., 2006). The V/(V+Ni) value increases linked to the increase in continental contribution. Additionally, oxic conditions are dominant at the time of aerobic microbial metabolic processes (JIANCHENG et al., 2006). If the V/(V+Ni) ratio is lower than 0.60, it indicates anoxic conditions at the time of mineralization (MARYNOWSKI et al., 2012). The ore sample V/(V+Ni) ratios were below 0.60 for 8 samples, but above 0.60 for 12 samples (Table 2). For this reason, oxic and anoxic conditions were dominant during mineralization occurring in the region. Additionally, sedimentary formation in a deep marine environment was effective on mineralization.

Elements like As, Cu, Mo, Pb, Sb, Sr, and V are enriched in hydrothermal fluids (NICHOLSON, 1992). When these elements are examined, enrichment was observed in all ore samples from the study area (Table 2).

Low Mo content in ferromanganese ore may reflect the low temperature of hydrothermal fluids (HEIN et al., 2008; ŞAŞMAZ et al., 2014). This value was 2.90–38.50 ppm (average 21.64 ppm) in the study area so mineralization in a low-temperature hydrothermal formation may be present (Table 2). The Co content in hydrothermal deposits is lower compared to hydrogenetic deposits. Hence, a high Co concentration is a marker of the deep marine environment (DEL RIO SALAS et al., 2008). This data reflects mineralization with a hydrothermal source in the study area.

Different major and trace element differentiation diagrams are used by many researchers for differentiation of manganese deposits with different sources (ADACHI et al., 1986; BONATTI et al., 1972; CHOI & HARIYA 1992; CRERAR et al., 1982; NICHOLSON, 1992; PETERS, 1988; SHAH & MOON, 2007; TOTH, 1980). These diagrams are used to differentiate between hydrothermal (continental or marine) and hydrogenetic sources. The term hydrothermal is used for manganese oxides deposited by sedimentary-exhalative manganese mineralization in marine environments or direct deposition from hot springs in pools and geothermal water in terrestrial environments (NICHOLSON, 1992). The term hydrogenetic is used for deposits formed by adsorption or slow precipitation of material dissolved in seawater (BONATTI et al., 1972; CRERAR et al., 1982; NICHOLSON, 1992). The geochemical data for ore samples from the study area were plotted on a Fe-(Ni+Co+Cu)x10-Mn ternary diagram (Fig. 7a; BONATTI et al., 1972). Accordingly, all samples were distributed in the hydrothermal field.

The source diagram determined with the Na/Mg ratio (NICHOLSON, 1992) showed that all samples were distributed in the freshwater field (Fig. 7b). The diagram of the Fe/Ti ratio against Al/(Al+Fe+Mn) was drawn (BOSTROM et al., 1976). Accordingly, the presence of a volcanic input into the mineralization processes was supported (Fig. 7c).

The  $\Sigma$ REE data obtained from ferromanganese samples had values from 2.70–62.70, an average of 28.00. Additionally, the LREE/HREE ratio in mineralized samples from the study area was 0.95–9.78 (ave 5.38) and this value shows enrichment in LREE values compared to HREE values. In hydrothermal solutions containing ore, HREEs are less stable than LREEs, so they primarily enrich LREE during manganese mineralization (RUHLIN & OWEN, 1986; ZARASVANDI et al., 2013). These  $\Sigma$ REE values show that the mineralization is compatible with hydrother-

mal deposits (e.g., Northeast Pacific Ocean Baby Bare Deposit; REE = 20.6–249.6 JIANCHENG et al., 2006), while they are very low compared to values from hydrogenetic deposits (e.g., Hazara deposit;  $\Sigma$ REE= 791 ppm; SHAH & MOON, 2007). It is known that the  $\Sigma$ REE contents of ferromanganese hydrothermal deposits are lower compared to the hydrogenous deposits (CHOI & HARIYA, 1992), while the  $\Sigma$ REE values of the hydrothermal oxide deposits have a wider range (MILLS et al., 2001; ŞAŞMAZ et al., 2014).

Formation environments display variability for Eu anomalies. The Eu value for seawater is 0.61 ppm, while the value is close to 7 ppm in hydrothermal deposits. Variations in Ce anomaly are close to 0.17 for seawater and 1.03 in the continental crust (DANIELSON et al., 1992; MANIKYAMBA & NAQVI, 1995; MISHRA et al., 2006; MORIYAMA et al., 2008). Ferromanganese samples from the study area had an Eu anomaly of 0.88–48.10 (ave. 9.94). The Ce anomaly value was 0.02–0.88 (ave. 0.58). When both anomalies are assessed, the effect of the mixing of seawater and hydrothermal fluids on mineralization may be considered. The positive Eu anomaly in mineralized samples is a typical feature of modern manganese hydrothermal deposits in the oceanic environment. Negative Ce anomaly shows the presence of oxic ocean water (WRIGHT et al., 1987; KOÇAK, 2020a, b). The REE data for mineralized samples in the study support the idea that manganese mineralization occurred as precipitation as a result of both hydrothermal solutions and mixing with seawater (DANIELSON et al., 1992; MANIKYAMBA & NAQVI, 1995; MISHRA et al., 2006; MORIYAMA et al., 2008).

When the  $Ce_{anom}$  values in the study area are noted, 15 samples had values lower than -0.1, while 5 samples had values larger than -0.1. These values show the environment had both oxic and anoxic characteristics. In mineralized samples, the Y/Ho ratio was determined as 33.29. This ratio is higher compared to hydrothermal solutions, so the presence of a hydrothermal source and continental derived environment may be suggested.

The histogram for homogenization temperatures measured in fluid inclusion studies of four samples is presented in Fig. 9. Three different quartz stages were identified in the measured samples and there are 3 different data intervals on the histogram for Th temperatures measured in fluid inclusions from these stages. Accordingly, the distribution of data on the histogram indicates 3 different solution stages.

Additionally, the eutectic temperatures for four samples are provided in Table 4. Accordingly, all samples had eutectic temperatures equivalent to different phases, ranging from -33.8 to -49.9 °C. When these eutectic temperatures are compared with the eutectic temperatures for different salt compositions given by SHEPHERD et al. (1985) (Fig. 10), all measurement results show fluid inclusion composition was comparable with H<sub>2</sub>O-CaCl<sub>2</sub>-NaCl-FeCl<sub>2</sub>-MgCl<sub>2</sub>.

While the salinity for Type I fluid inclusions varies from 1.9 to 14.7 wt.% NaCl equiv., Type II and III fluid inclusions had lower salinity values of 1.9 to 5.1 wt.% NaCl equiv. Accordingly, the Th-salinity trend for Type I fluid inclusions was compatible with a dilution trend for hydrothermal solutions with surface solutions (Fig. 11). This trend indicates that solutions with the partly high salinity in Type I fluid inclusions (may have a magmatic source) mixed with solutions with low salinity (meteoric). In contrast, Type II and III fluid inclusions had salinities from 1.9 to 5.1 wt.% NaCl equiv. which indicate they formed under the effect of meteoric solutions.

## 7. CONCLUSIONS

1. As a result of field studies, geochemical and petrographic investigations, and fluid inclusion studies, mineralization may be considered to have formed in three stages.
2. Additionally, the formation occurred by ferromanganese mineralization precipitating in both oxic and anoxic environments with hydrothermal solutions affected by mixing with seawater.
3. According to fluid inclusion studies, the three different solution stages of mineralization can be said to have temperatures of 338–438 °C for the first stage, 269–317 °C for the second stage, and 143–236 °C for the third stage. The calculated salinity concentrations were particularly high for Type I fluid inclusions (1.9–14.7 wt.% NaCl equiv.) and lower for Type II and III fluid inclusions (1.9–5.1 wt.% NaCl equiv.). Decreasing salinity versus the Th temperature trend in Figure 11. indicates that mineralization formed from a mixture of magmatic and meteorically derived solutions.
4. In the mineralized samples, the Y/Ho ratio (33.29) is higher compared to hydrothermal solutions, so the presence of a hydrothermal source and continental derived environment may be suggested.
5. Apart from two samples, all the ore samples had a Sr/Ba ratio lower than 1 representing formation in a continental sedimentary environment for mineralization in the study area.
6. In the region, magmatism developed in the form of plutonic activity within crystalline massifs and as submarine volcanism in the Upper Cretaceous and Middle Eocene periods. Later it is thought there was variation in ore minerals with the effect of meteoric waters. In the study area, the first phase of mineralization with three different phases of bands and stockwork structure at the basalt-limestone contact and within limestones is thought to have formed with volcanic activity in the Middle Eocene period.

## ACKNOWLEDGMENT

This study constitutes part of the MSc., thesis of Sümeyra KAYA and the project with the code number 6601-FBE/19-332, supported by Yozgat Bozok University.

## REFERENCES

- ADACHI, M., YAMAMOTO, K. & SUGISAKI, R. (1986): Hydrothermal chert and associated siliceous rocks from the northern Pacific: their geological significance as indication of ocean ridge activity.— *Sedimentary Geology*, **47**, 125–148.
- AKÇAY, A.E., DÖNMEZ, M., KARA, H., YERGÖK, A.F. & ESENTÜRK, K. (2007): Turkish Geological Maps Series with a scale of 1/100000, Yozgat-i33 Map. MTA, Ankara, 80, 1–16. (in Turkish)
- BAU, M. & DULSKI, P. (1999): Comparing yttrium and rare earths in hydrothermal fluids from the mid-atlantic ridge: Implications for Y and REE behaviour during near-vent mixing and for the Y/Ho ratio of proterozoic seawater.— *Chemical Geology*, **151**–2, 77–90. doi:10.1016/S0009-2541(98)00142-9
- BODNAR, R.J. (1993): Revised equation and table for determining the freezing point depression of H<sub>2</sub>O–NaCl solutions.— *Geochim. Cosmochim. Acta* **57**, 683–684. doi: 10.1016/0016-7037(93)90378-A
- BONATTI, E., KRAEMER, T. & RYDEL, H. (1972): Classification and genesis of submarine iron-manganese deposits.— In: HORN, D.R. (ed.): *Ferromanganese deposits on the ocean floor*.— National Science Foundation, 149–166.
- BOLHAR, R., KAMBER, B.S., MOORBATH, S., FEDO, C.M. & WHITEHOUSE, M.J. (2004): Characterisation of early Archaean chemical sediments by trace element signatures.— *Earth and Planetary Science Letters*, **222**, 43–60. doi: 10.1016/j.epsl.2004.02.016
- BOSTROM, K., JOENSUU, O., VALDES, S., CHARM, W. & GLACCUM, R. (1976): Geochemistry and origin of east pacific sediments sampled during DSDP leg 34.— In: YEATS, R.S. & HART, A.S.R. (eds.): *Initial reports of the deep sea drilling project*. 34, 556–574, U.S. Government Printing Office. doi: 10.2973/dsdp.proc.34.149.1976
- CHOI J.H. & HARIYA, Y. (1992): Geochemistry and depositional environment of Mn oxide deposits in the Tokora Belt, Northeastern Hokkaido, Japan.— *Economic Geology*, **87**, 12. doi: 10.2113/gsecongeo.87.5.1265
- CONLY, A.G., SCOTT, S.D., & BELLON, H. (2011): Metalliferous manganese oxide mineralization associated with the Boléo Cu-Co-Zn district, Mexico.— *Economic Geology*, **106**/7, 1173–1196. doi: 10.2113/econgeo.106.7. 1173
- CRERAR, D.A., NAMSON, J., CHYL, M.S., WILLIAMS, L. & FEIGENSON, M.D. (1982): Manganiferous cherts of the Franciscan assemblage: I. General geology, ancient and modern analogues, and implications for the hydrothermal convection at oceanic spreading centres.— *Economic Geology*, **77**, 519–540. doi: 10.2113/gsecongeo.77.3.519
- DANIELSON, A., MÖLLER, P. & DULSKI, P. (1992): The Europium anomalies in banded iron formations and the thermal history of the oceanic crust.— *Chemical Geology*, **97**, 89–100. doi: 10.1016/0009-2541(92)90137-T
- DELIAN, F. (1994): *Geological and Geochemical Research of the Manganese ore Bed (in Chinese)*, M1. Weather Publishing Press, Beijing.
- DEL RIO SALAS, R., RUIZ, J., OCHOA-LANDÍN, L., NORIEGA, O., BARRA, F., MEZA-FIGUEROA, D. & PAZ-MORENO, F. (2008): Geology, Geochemistry and Re-Os systematics of manganese deposits from the Santa Rosalia Basin and adjacent areas in Baja California Sur, México.— *Mineralium Deposita*, **43**/4, 467–482. https://doi.org/10.1007/s00126-008-0177-3
- DOE, B.R., AYUSO, R.A., FUTA, K. & PETERMAN, Z.E. (2013): Evaluation of the sedimentary manganese deposits of Mexico and Morocco for determining lead and strontium isotopes in ancient seawater.— In: BASU, A. & HART, S. (eds.): *Earth Processes: Reading the Isotopic Code*. (1996), *Geophys. Monogr. Ser.*, vol. 95, 391–408. doi: 10.1029/GM095p0391
- EVENSEN, M.N., HAMILTON, P. & O'NIONS, R.K. (1978): Rare-earth abundances in chondritic meteorites.— *Geochim. Cosmochim. Acta*, **42**, 1199–1212. doi: 10.1016/0016-7037(78)90114-X
- FERNANDEZ, A. & MORO, M.C. (1998): Origin and depositional environment of Ordovician stratiform iron mineralization from Zamora (NW Iberian Peninsula).— *Mineralium Deposita*, **33**, 606–619. doi: 10.1007/s001260050176
- GÖYMEN, G. & KOÇ, Ş. (2000): *Ore Microscopy*.— Ankara University Science Faculty Publish, 60.
- GÜLTEKİN, A.H. (1998): Geochemistry and origin of the Oligocene Binkılıç manganese deposit, Thrace basin, Turkey.— *Turkish Journal of Earth Sciences*, **7**, 11–24.
- HAYASHI, K.I., FUJISAWA, H., HOLLAND, H.D. & OHMOTO, H. (1997): Geochemistry of 1.9 Ga sedimentary rocks from northeastern Labrador, Canada.— *Geochimica et Cosmochimica Acta*, **61**/19, 4115–4137. doi: 10.1016/S0016-7037(97)002147
- HEIN, J.R., SCHULZ, M.S., DUNHAM, R.E., STERN, R.J. & BLOOMER, S.H. (2008): Diffuse flow hydrothermal manganese mineralization along the active Mariana and Southern Izu-Bonin arc system, Western Pacific.— *Journal of Geophysical Research*, **113**, B08, 14. doi: 10.1029/2007JB005432
- JIANCHENG, X., XIAOYONG, Y. & JIANGUO, D. (2006): Geochemical Characteristics of Sedimentary Manganese Deposit of Guichi, Anhui Province, China.— *Journal of Rare Earths*, **24**, 374–380. doi: 10.1016/S1002-0721(06)60127-0
- KARAKUŞ, A., YAVUZ, B. & KOÇ, Ş. (2010): Mineralogy and major trace element geochemistry of the Haymana manganese Mineralizations, Ankara, Turkey.— *Geochemistry International*, **48**, 1014–1027. doi: 10.1134/s001670291010006x
- KATO, Y., YAMAGUCHI, K.E. & OHMOTO, H. (2006): Rare earth elements in Precambrian banded iron formations: secular change of Ce and Eu anomalies and evolution of atmospheric oxygen.— *Geological Society of America Bulletin*, **118**, 269–289. doi: 10.1130/2006.118(16)
- KETIN, I. (1955): The geology of the Yozgat region and the tectonic situation of the Central Anatolian Massif.— *The Bulletin of the Geological Society of Turkey*, **6**/1, 1–40.
- KETIN, I. (1966): Tectonic units of Anatolia.— *Bulletin of the Mineral Research and Exploration Institute*, **66**, 20–34.
- KHAN, M.A., KAKAR, M.I., ULRICH, T., ALI, L., KERR, A.C., MAHMOOD, K. & SIDDIQUI, R.H. (2020): Genesis of Manganese Deposits in the Ali Khanzai Block of the Zhoob Ophiolite, Pakistan: Inferences from Geochemistry and Mineralogy.— *Journal of Earth Science*, **31**/5, 884–895. doi: 10.1007/s12583-020-1337-3
- KOÇAK, I. (2020a): Sarhıdır manganese mineralization related to travertine, Central Anatolian Volcanic Province, Turkey.— *Geodinamica Acta*, **32**/1, 11–24. doi: 10.1080/09853111.2020.1829904
- KOÇAK, I. (2020b): Geochemistry of the Igdekoy-Doganlar Na-Ca borate deposit, Emet Province (western Anatolia, Turkey).— *Geological Quarterly*, **64**/3, 807–817. doi: 10.7306/gq.1555
- KOÇ, Ş., ÖZMEN, Ö. & ÖKSÜZ N. (2000): Geochemistry characteristic of Kasimaga (Keskin-Kırkkale) manganese oxide mineralizations.— *Mineral Research and Exploration magazine*, **122**, 107–120.
- KRAUSKOPF, K.B. (1989): *Introduction to Geochemistry*.— McGraw-Hill International Editions, Auckland.
- MANIKYAMBA, C. & NAQVI, S.M. (1995): Geochemistry of Fe-Mn formations of the Archean Sandur schist belt, India -- mixing of clastic and chemical processes at a

- shallow shelf.– *Precambrian Research*, 72, 69–95. doi: 10.1016/0301-9268(94)00050-2
- MARYNOWSKI, L., ZATOŃ, M., RAKOCIŃSKI, M., FILIPIAK, P., KURKIEWICZ, S. & PEARCE, T.J. (2012): Deciphering the upper Famennian Hangenberg Black Shale depositional environments based on multi-proxy record.– *Palaeogeogr. Palaeoclimatol. Palaeoecology*, 347, 66–86. doi: 10.1016/j.palaeo.2012.05.020
- MILLS, R.A., WELLS, D. & ROBERTS, S. (2001): Genesis of ferromanganese crusts from the TAG hydrothermal field.– *Chemical Geology*, 176, 3–293. doi: 10.1016/S0009-2541(00)00404-6
- MISHRA, P., MOHAPATRA, B.K. & SINGH, P.P. (2006): Mode of occurrence and characteristics of Mn-ore bodies in Iron Ore Group of rocks, North Orissa, India and its Significance in Resource Evaluation.– *Resource Geology*, 56, 55–64. doi: 10.1111/j.1751-3928.2006.tb00268.x
- MONNIN, C., WHEAT, C.G., DUPRE, B., ELDERFIELD, H. & MOTTL, M.J. (2001): Barium geochemistry in sediment pore waters and formation waters of the oceanic crust on the eastern flank of the Juan de Fuca Ridge (ODP Leg 168).– *Geochem. Geophys. Geosyst.*, 2/1, 1008–1023. doi: 10.1029/2000GC000073
- MORIYAMA, T., PANIGRAHI, M.K., PANDIT, D. & WATANABE, Y. (2008): Rare earth element enrichment in Late Archean manganese deposits from the Iron Ore Group, East India.– *Resource Geology*, 58, 402–413. doi: 10.1111/j.1751-3928.2008.00072.x
- NAREJO, A.A., SHARI A.M., FATIMA, N. & SOHAIL, K. (2019): Geochemistry and origin of Mn deposits in the Bela ophiolite complex, Balochistan, Pakistan.– *Journal of Petroleum Exploration and Production Technology*, 9, 2543–2554. doi: 10.1007/s13202-019-0742-6
- NAYAN, J., RONGFEN, J. & ZIYU, W. (1994): Permian palaeogeography and geochemical environment in Lower Yangtze region, China.– *Petroleum Industry Press, Beijing*, 206.
- NICHOLSON, K. (1992): Genetic Types of Manganese Oxide Deposits in Scotland: Indicators of Paleo Ocean Spreading Rate and a Devonian Geochemical Mobility Boundary.– *Economic Geology*, 87, 1301–1309. doi: 10.2113/gsecongeo.87.5.1301
- NICHOLSON, K., NAYAK, V.K. & NANDA J.K. (1997): Manganese ores of the Ghorajhor-Monmunda area, Sundergarh District, Orissa, India: Geochemical evidence for a mixed Mn source.– *Geological Society, Special Publications*, 119/1, 117. doi: 10.1144/GSL.SP.1997.119.01.08
- OKTAY, F.Y. (1981): The geology of the sedimentary cover of the Central Anatolian Massif around Savcılı-Büyükkoba (Kaman).– ITU Faculty of Mining. Associate Professor thesis, Istanbul.
- OSTWALD, J. (1984): Two varieties of lithiophorite in some Australian deposit.– *Mineral. Mag.*, 48, 383–388. doi: 10.1180/minmag.1984.048.348.08
- ÖKSÜZ, N. (2011a): Geochemical characteristics of the Eymir (Sorgun-Yozgat) manganese deposit, Turkey.– *Journal of Rare Earths*, 29/3, 287–296. doi: 10.1016/S1002-0721(10)60446-2
- ÖKSÜZ, N. (2011b): Geochemistry and the origin of manganese mineralizations in Derbent (Yozgat) Region.– *Bulletin of the Earth Sciences Application and Research Centre of Hacettepe University*, 32/3, 213–234 (in Turkish)
- ÖKSÜZ, N. (2018): Mineralogical findings from manganese deposits in the artova ophiolite complex, Derbent-Eymir area, Yozgat, Turkey.– *Bulletin of the Mineral Research and Exploration*, 156, 137–150. doi: 10.19111/bulletinofmre.334245
- ÖKSÜZ, N., KOÇAK, İ. & TEMİZ, U. (2021): Geochemical and tectonic characteristics of manganese mineralization in the Yozgat region, Turkey.– *Geological Quarterly*, 65/2, 31. doi: 10.7306/gq.1599
- ÖKSÜZ, N. & OKUYUCU, N. (2014): Mineralogy, geochemistry, and origin of Buyukmahal manganese mineralization in the Artova ophiolitic complex, Yozgat, Turkey.– *Journal of Chemistry*, 837972. doi: 10.1155/2014/837972
- ÖZCAN, A., ERKAN, A., KESKİN, E., ORAL A., OZER, S., SUMENGEN, M. & TEKELİ, O. (1980): The basic geology of the North Anatolian Fault-Kırşehir Massif. Ankara.– *Bulletin of the Mineral Research and Exploration report number: 6722* (unpublished; in Turkish)
- ÖZTÜRK, H. (1993): Manganese mineralizations in Turkey: Processes of formation and types.– *Istanbul University Eng. Fac. Geological Engineering Pub.*, 43, 24.
- PETERS, T. (1988): Geochemistry of manganese-bearing cherts associated with Alpine ophiolites and the Hawasina formations in Oman.– *Marine Geology*, 84/3–4, 229–238. doi: 10.1016/0025-3227(88)90103-X
- PLANAVSKY, N., BEKKER, A.J., ROUXEL, O., KAMBER, B., HOFMANN, A., KNUDSEN, A.G. & LYONS, T.W. (2010): Rare Earth Element and yttrium compositions of Archean and Paleoproterozoic Fe formations revisited: New perspectives on the significance and mechanisms of deposition.– *Geochimica et Cosmochimica Acta*, 74, 6387–6405. doi: 10.1016/j.gca.2010.07.021
- POLGÁRI, M., HEIN, J.R., VIGH, T., SZABÓ-DRUBINA M., FÓRIZS, I., BÍRÓ L., MÜLLER, A. & TOTH A.L. (2012): Microbial processes and the origin of the Úrkút manganese deposit.– *Hungary Ore Geol. Rev.*, 47, 87–109. doi:10.1016/j.oregeorev.2011.10.001
- RAMDOHR, P. (1980): *The Ore Minerals and Their Intergrowth.*– Pergamon Press, Oxford, London, New York.
- ROEDDER, E. (1984): *Fluid inclusions. Reviews in Mineralogy.*– Mineralogical Society of America, Washington, 12, 644.
- RUHLIN, D.E. & OWEN, R.M. (1986): The rare earth element geochemistry of hydrothermal sediments from the East Pacific Rise: examination of a seawater scavenging mechanism.– *Geochimica et Cosmochimica Acta*, 50, 393–400. doi: 10.1016/0016-7037(86)90192-4
- SCHWARTZ, G.M. (1951): Classification and definitions of textures and mineral structures in ores.– *Economic Geology*, 46, 578–591. doi: 10.2113/gsecongeo.46.6.578
- SEYMEN, I. (1982): *The geology of the Kırşehir Massif around Kaman (Kırşehir).*– ITU Faculty of Mining. Associate Professor Thesis (unpublished), 164, İstanbul.
- SHAH, M.T. & MOON, C.J. (2007): *Manganese And Ferromanganese Ores From Different Tectonic Settings.* In *The NW Himalayas, Pakistan.*– *Journal of Asian Earth Sciences*, 29, 455–465. doi: 10.1016/j.jseaes.2005.11.002
- SHEPHERD, T.J., RANKIN, A.H. & AIDERTON, D.H.M. (1985): *A Practical Guide to Fluid Inclusion Studies.*– Blackie and Son Limited, Glasgow (U.K.), 235.
- SUGITANI, K., HORIUCHI, Y., ADACHI, M. & SUGISAKI, R. (1996): Anomalously low Al<sub>2</sub>O<sub>3</sub>/TiO<sub>2</sub> values for archean cherts from the pilbara block, Western Australia - possible evidence for extensive chemical weathering on the early earth.– *Precambrian Research*, 80/1–2, 49–76. doi: 10.1016/s0301-9268(96)00005-8
- SYLVESTREA, G., TIMOLEONA, N., NONO, K., DJIBRILA, G., JEAN, P.N. & MARIANNE, N.F. (2015): Petrology and geochemistry of the banded iron-formations from Ntem complex greenstones belt, Elom area, Southern Cameroon: Implications for the origin and depositional environment.– *Chemie der Erde*, 75, 375–387. doi: 10.1016/j.chemer.2015.08.001
- ŞAŞMAZ, A., TÜRKYLMAZ, B., ÖZTÜRK, N., YAVUZ, F. & KUMRAL, M. (2014): Geology and geochemistry of Middle Eocene maden complex ferromanganese deposits from Elazığ-Malatya Region, Eastern, Turkey.– *Ore Geology Reviews*, 56, 352–372.
- TOTH, J.R. (1980): Deposition of submarine crusts rich in manganese and iron.– *Geol. Soc. America Bul.*, 91/1, 44–54. doi: 10.1130/0016-7606(1980)91%3C44:DOSCR1%3E2.0.CO;2
- WRIGHT, J., SCHRADER, H. & HOLSER, W.T. (1987): Paleoredox variations in ancient oceans recorded by rare-earth elements in fossil apatite.– *Geochim Cosmochim Acta*, 51, 631–644. doi: 10.1016/0016-7037(87)90075-5
- XIE, J.C., YANG, X.Y., DU, J.G. & XU, W. (2006): Geochemical characteristics of sedimentary manganese deposit of Guichi, Anhui Province, China.– *J. Rare Earths*, 24/3, 374–380. doi: 10.1016/S1002-0721(06)60127-0
- XU, B., DING, S., WANG, Y. & LIU, Q. (2011): Geochemical characteristics of illite clay rocks from the Shihezi formation in the hanxing mining area and its sedimentary environment.– *Mining Science and Technology*, 21/4, 495–500. doi: 10.1016/j.mstc.2011.06.006
- ZARASVANDI, A., LENTZ, D., REZAI, M. & POURKASEB, H. (2013): Genesis of the Nasirabad manganese occurrence, Fars province, Iran: Geochemical evidences.– *Chemie der Erde-Geochemistry*, 73, 495–508. doi: 10.1016/j.chemer.2013.02.003
- ZARASVANDI, A., POURKASEB, H., SEPAHVAND, M.R., RAIH, J. & REZAEI, M. (2016): Tracing of hydrothermal ore forming process in the Sorkhvand manganese deposit, Kermanshah Province, Iran.– *Arabian Journal of Geoscience*, 9, 109–123. doi: 10.1007/s12517-015-2237-1